NASA TECHNICAL MEMORANDUM NASA TM-76648

AERODYNAMIC INVESTIGATIONS TO DETERMINE POSSIBLE ICE FLIGHT PATHS

W. Burgsmueller, H. Franz, P. May and G. Anders

(NASA-TM-76648) AERODYNAMIC INVESTIGATIONS TO DETERMINE POSSIBLE ICE FLIGHT PATHS (National Aeronautics and Space Administration) 77 p HC A05/MF A01 CSCL 01C

N82-27235

Unclas
G3/03 28233

Translation of
"Aerodynamische Untersuchungen zur Feststellung möglicher Eisflugbahnen", Bremen, West Germany, Vereinigte Flugtechnische Werke-Fokker GMBH, Report Ef-586 (in 4 parts), part 1 (20 pages), part 2 (8 pages), part 3 (50 pages), part 4 (5 pages), January 18, 1977, 84 pages.

NATIONAL AERONAUTICS AND SPACE ADMINISTRATION
WASHINGTON, DC 20546 MARCH 1982

STANDARD TITLE PAGE

1. Report No. NASA TM-76648	2. Government Accession No.	3. Recipient's Catalog No.
4. Title and Subtitle: Aerodynamic Investigations to Determine Possible Ice Flight Paths		5. Report Date: March 1982 6. Performing Organization Code
7. Author(s): W. Burgsmueller, H. Franz, P. May, G. Anders.		8. Performing Organization Report No. 10. Work Unit No.
9. Performing Organization Name and Address: Leo Kanner Assoc., Redwood City, CA 94063		11. Contract or Grant No. NASw-3541 13. Type of Report and Period Covered: Translation
12. Sponsoring Agency Name and Address: National Aeronautics and Space Administration Washington, DC 20546		14. Sponsoring Agency Code

15. Supplementary Notes

Translation of "Aerodynamische Untersuchungen zur Feststellung möglicher Eisflugbahnen", Bremen, West Germany, Vereinigte Flugtechnische Werke--Fokker GMBH, Report Ef-586 (in 4 parts), part 1 (20 pages), part 2 (8 pages), part 3 (50 pages), part 4 (5 pages), January 18, 1977, 84 pages.

16. Abstract

After flights with the VFW 614 under severe icing conditions, damage to the engines was found.

In wind tunnel tests a determination of the origin of this ice was made--it is supposed that the damage was caused by this ice. On the modified flight test model of the VFW 614 on a 1:15 scale, measurements were conducted in the VFW-Fokker wind tunnel from 11/28 to 12/9/75 with exposed particles which represented the free ice.

The results of this testing are presented in this report.

17. Key Words (Selected by Author(s))	18. Distribution Statement: Unclassified-Unlimited		
19. Security Classif. (of this report): Unclassified	20. Security Classif. (of this page): Unclassified	21. No. of Pages	22.

NASA-HQ

Vereinigte Flugtechnische Werke (VFW) Fokker, GmbH, Report Ef 21

Summary

After flights with the VFW 614 under severe icing conditions, damage to the engines was found.

In wind tunnel tests, a determination of the origin of this ice was made--it is supposed that the damage was caused by this ice. On the modified flight test model of the VFW 614 on a 1:15 scale, measurements were conducted in the VFW-Fokker wind tunnel from 11/28 to 12/9/75 with exposed particles which represented the free ice.

The results of this testing are presented in this report. The report consists of 4 parts:

Part 1: Calculations of path, as a preliminary consideration for critical ice generation (W. Burgsmüller)

Part 2: Similarity laws, as preparation for wind tunnel tests with ice release (H. Franz)

Part 3: Measurement Report, Description of the set-up, Implementation and results (P. May)

Part 4: Summary of Results (G. Anders)

Verteiler / Copy to:		Neuausgabe / Re-issue:	Datum / Date:	Bem. / Remarks:
Herren		Zusammenfassung	18.1.1977	
Schüffler	E			
Kathen	Eo 2			
Issel	Ev 12			
Rummel/Held	Ek 244			
Krenz	Ef 1	And.-Ausg. / Revision:	Seite / Page: Datum / Date:	
Ewald	Ei 2			
Anders	Ef 22			
Franz	Ef 21			
Burgsmüller	Ef 22			
May	Ef 21			

REPORT Ef 586, Part 1

Subject: Approximation Calculation of the Path of an Ice Chunk Broken Off the Nose of the VFW 614

Summary: By means of an approximation calculation it shall be checked whether the ice chunks sent into the engine of the VFW 614 in flight originated at the nose of the aircraft.

The computation results show that for a positive angle of incidence of 3 - 4° in the upper nose region, separating ice follows paths leading either directly into the engine or to its direct vicinity. It is therefore possible that the source of the engine damage is due to icing of the fuselage nose.

Bearbeitet / Prepared	Geprüft / Checked	Gebilligt / Approved	Anerkannt / Acknowledged
[signature]		[signature]	

Verteiler / Copy to:	Neuausgabe / Re-issue: Datum / Date:	Bem. / Remarks:
	Änd.-Ausg. / Revision: Seite / Page: Datum / Date:	
Datum/Date: 8.12.75 Ausg./Rev.No.:		Anz. der Seiten: 20 Numb. of Pages:

Contents

List of Figures

Figures

1. Introduction

In a preliminary investigation it was to be determined whether it would be possible for ice chunks breaking off the fuselage nose of the VFW 614 to get into the engine.

The calculation was initially performed for $\alpha = 0\,^{\circ}$ and four different-size ice cubes. In order to do this, the pressure distribution on the fuselage-side was determined from a wind tunnel measurement. The assumptions on which the calculation are based are:

-incompressible and
-fuselage-parallel streaming in all considered sections.

The same assumptions were made in two additional computations which were designed to explain the influence of the angle between fuselage axis and ice chunk, and the angle of incidence.

2. Flight Data

The following flight data serves as input values for the path calculation:

-altitude: 1000-2000 m
-velocity: 200 kn CAS
-angle of incidence: $3\text{-}4^{\circ}$
-temperature: $0\,^{\circ}C$

From this data results an average stagnation pressure of $q_{H_\infty} = 650\ kp/m^2$ (index H = full-scale design).

3. Path Assumptions

Regarding the path of the ice chunk, the following simplifying assumptions are made:

-the ice chunk breaks off from the middle of the nose
-the path from the nose to the engine is broken into three segments (S_1 - S_3)(see fig. 1):

S_1 = radius of the nose
S_2 = cone
S_3 = parallel piece

-up to the end of the 2nd segment, the path of the ice chunk in the x-y plane, is parallel to the fuselage wall; there it releases parallel to the cone section at a 25^{o} angle to the fuselage longitudinal axis.

4. Assumptions about the Ice Chunks

-The calculation is performed for 4 cases with ice cubes of 1, 2, 3 and 4 cm edge length

-At a density of 1 g/cm^3, the masses are 1, 8, 27 and 64 g.

-The reference surfaces used to determine resistance are 1, 4, 9 and 16 cm^2--regardless of the particular streaming direction.

-The coefficient of resistance is in all cases $C_W = 0.7$.

5. Simplified Assumptions Regarding the Local Air Velocities

-First, the c_p-values of a wind tunnel measurement were converted into stagnation pressures under flight conditions (see diagram 1)

-In order to simplify the calculations, the average stagnation pressures were determined from this for the individual computation segments, and from this again, the average air velocities were determined.

We have:

$q_{m_{S_1}} = 400\ kp/m^2$ $\quad v_{m_1} = 85{,}28\ m/s$

$q_{m_{S_2}} = 750\ kp/m^2$ $\quad v_{m_2} = 116{,}8\ m/s$

$q_{m_{S_{31}}} = 800\ kp/m^2$ $\quad v_{m_{31}} = 120{,}6\ m/s$

$q_{m_{S_{32}}} = q_{m_{S_{33}}} = 650\ kp/m^2$ $\quad v_{m_{32}} = v_{m_{33}} = v_\infty = 108{,}7\ m/s$

-As a simplification, it was assumed that the streaming has no z-component and is directed parallel to the local fuselase wall (nose or cone) in segments S_1 and S_2, but is parallel to the fuselage in segment S_3

-The air density was set in accord with the flight altitude as
$\varrho = 1{,}079\ kg/m^3$
-The angle of incidence is $\alpha = 0\ °$.

6. Used Equations

6.1 Designations

F	$[m^2]$	Reference surface of the particular ice chunk
m	[kg]	Mass of the particular ice chunk
$S_{1,2,3}$	[m]	Length of the fuselage contour line in the particular computation section (measured in the x-y plane)
s	[m]	Path covered in time t in the streaming direction by the ice chunk (aircraft-specific)
$s_{x,y,z}$	[m]	Components of path covered by the ice chunk in time t in the x, y, z-system
t	[sec]	Time
t_o	[sec]	Time at the beginning of the particular computation section
$v_{m_{1,2,3}}$	[m/s]	Average streaming velocity of the air in the particular computation section relative to the aircraft (Direction always parallel to the fuselage contour and in the x, y-plane
w	[m/s]	Velocity of the ice chunk in the streaming direction at time t (aircraft-specific)
w_x, w_y, w_z	[m/s]	Components of velocity of the ice chunk at time t in the x, y, z-system
ϱ	$[kg/m^3]$	Density of the air

Indices

∞ Conditions in the direction of air flow

o State at the beginning of the particular calculation segment

6.2 General Information

The total instantaneous force acting on the ice chunk is composed of one component parallel to the local air flow and one component perpendicular to it. In the case considered here, the perpendicular component can again be broken down into one acting in the horizontal plane of the aircraft (x, y-plane) and one directed perpendicularly downward (x, z-plane). In the case under examination here, it can be assumed that the path angle of the aircraft is $\vartheta = 0°$ i.e. the z-direction of the aircraft-specific reference system coincides with the direction of the acceleration of gravity.

The force components have the following effect on the ice chunk:

-In the streaming direction, it is accelerated due to its own resistance and to the difference of streaming and inherent velocity

-An inherent speed present in the x, y-plane perpendicular to the initial direction of air flow is retarded due to the resistance of air.

-In the vertical direction, gravity and air resistance act to accelerate or retard, respectively.

6.3 Calculation of Components in the Streaming Direction

The change in velocity of the ice chunk in the streaming direction results from the equation:

$$m \frac{d_w}{d_t} = \frac{C_w \cdot F \cdot \rho}{2} (v_m - w)^2 \qquad (1)$$

If we assume that at time t = 0 the speed of the ice chunk is $w = w_o$, then from (1) after a single integration, we have:

$$w = v_m - \frac{1}{\frac{1}{v_m - w_o} + \frac{C_w F \rho}{2m} \cdot t} \qquad (2)$$

This generates a relation between the time and instantaneous velocity of the ice chunk in the flow direction. But since we know the initial conditions v_m and w_o and the path s covered in the flow direction in the particular section, but not the time needed for this, equation (2) must be integrated again.

Proceeding from $w = \frac{ds}{dt}$ and the boundary condition $t = 0: s = 0$ it follows then:

$$s = v_m \cdot t - \frac{2m}{C_w F \varrho} \left[\ln \left(\frac{1}{v_m - w_o} + \frac{C_w F \varrho}{2m} \cdot t \right) - \ln \frac{1}{v_m - w_o} \right] \quad (3)$$

From this equation, the time needed for the path s is determined by iteration. Since the streaming is always parallel to the fuselage in the x, y-plane, s = S always, or in the computation section S_3, we have $s_3 = s_{3_x} = S_{3_x}$.

With the result from (3), the velocity of the ice chunk in the streaming direction can be determined from (2) at the end of the particular computation segment.

6.4 Calculation of Components Perpendicular to the Streaming Direction

6.4.1 Diagonal Components in the x-, y-plane

Since the path of the ice chunk in sections S_1 and S_2 is always parallel to the fuselage or streaming according to our assumptions, then the following calculations must be applied in section S_3. The air streaming in section S_3 is fuselage-parallel and thus parallel to the x-axis of the aircraft. The velocity w_2 of the ice chunk at the end of S_2 or the beginning of S_3, which was flow-parallel in S_2, must be broken down into an x- and y-component in section S_{31} relative to the streaming direction there. Thus, the ice chunk at the beginning of the section S_{31} has a velocity component W_{31_y} diagonal to the incident flow $v_{m_{31}}$. This initial velocity w_{31_y} is then reduced in this section due to the air resistance during the flight.

The desired velocity $w_y(t)$ results through integration as:

$$m \frac{dw_y}{dt} = - \frac{C_w F \rho}{2} w_y^2 \qquad (4)$$

with the boundary condition

$$t = 0 : w_y = w_{y_o}$$

$$w_y = \frac{1}{\frac{1}{w_{y_o}} + \frac{C_w F \rho}{2m} t} \qquad (5)$$

The time t is taken from equation (3), i.e. the speed in the y-direction is determined at the end of the computation segment.

To determine the flight path of the ice chunk relative to the aircraft, it is necessary to compute the traversed distance s_y within the computed time in the y-direction relative to the aircraft.

This is obtained by another integration of equation (5) with the boundary condition $t = 0 : s_y = s_{y_o}$:

$$s_y = \frac{2m}{C_w F \rho} \left[\ln \left(\frac{1}{w_{y_o}} + \frac{C_w F \rho}{2m} . t \right) - \ln \frac{1}{w_{y_o}} \right] \qquad (6)$$

6.4.2 Diagonal Components in the x-, z-plane

In a computation of these components, the air resistance is neglected since the influence along the path in the z-direction is less than 1%. By means of the gravitation law and the time t determined from equation (3), the z-components of the ice chunk become:

$$w_z = w_{z_o} + g . t \qquad (7)$$

and from this, for $t = 0$: $s_z = s_{z_o}$:

$$s_z = s_{z_o} + \frac{g}{2} t^2 \qquad (8)$$

7. Calculation

-Specify the parameters of the ice chunk: m, F, C_w

-Determine the air density ϱ

-Compute the constant $\frac{2m}{C_w F \varrho}$

-Average the average stagnation pressure of the streaming over the path length S from diagram 1 and determination of v_m from this.

-Insert initial velocity of the ice chunk w_o

-Determine the time t belonging to the transit length s by iteration from equation (3)

-By inserting t into equation (2), compute the velocity of the ice chunk in the streaming direction reached at the end of transit length s

-In segment S_3, determine the velocity w_y and the path s_y from equations (5) and (6)

-Compute the vertical components s_z and w_z from equation (7) and (8).

8. Results

The results of the path calculations for $\alpha = 0^\circ$ are found in figs. 2 to 5. In order to determine the influence of the angle of departure at the end of the segment S_2, in an additional calculation it was assumed that the ice chunk loosens not at a 25° angle, but at a 23° angle from the fuselage, i.e. the follows the fuselage curvature somewhat farther. The result of the calculation is shown in fig. 6.

For the sake of simplicity, all path calculations were conducted for $\alpha = 0^\circ$. Since the flight on which the calculations are based took place at an angle of incidence of $\alpha = 3 - 4^\circ$, in one case, the path curve for $\alpha = 4^\circ$ was determined and presented in fig. 7.

The influence of the wind on the streaming field was neglected in the approximation calculation described here. From an estimation we do find that this streaming field at $\alpha = 0^\circ$ in cases 1 and 2 (fig. 2, 3) and at $\alpha = 4^\circ$ in all cases (fig. 2 - 5) would lift up the path of the ice chunk in the direction of the engine inlet.

9. Conclusions

From the paths illustrated in figs. 2 to 7, we find:

-For the x-y-plane:

-The influence of the size of the ice chunk is low (larger pieces move on paths shifted toward the fuselage

-The influence of the angle of departure from the fuselage at the end of segment S_2 is very great (2° angle change causes 18 cm y-difference in the engine plane)

-The paths lead directly past the outer edge of the engine or directly into the engine, depending on angle of departure.

-For the x-z-plane:

-The influence of the ice chunk size is very great (larger pieces = lower paths)

-The quadrant angle of departure and the elevation of the place from which the ice chunk splits off, likewise have a great influence.

-The path calculations show that it is quite possible that a chunk of ice splitting off from the upper nose region at an angle of incidence of 3 to 4°, will be accelerated into the engine.

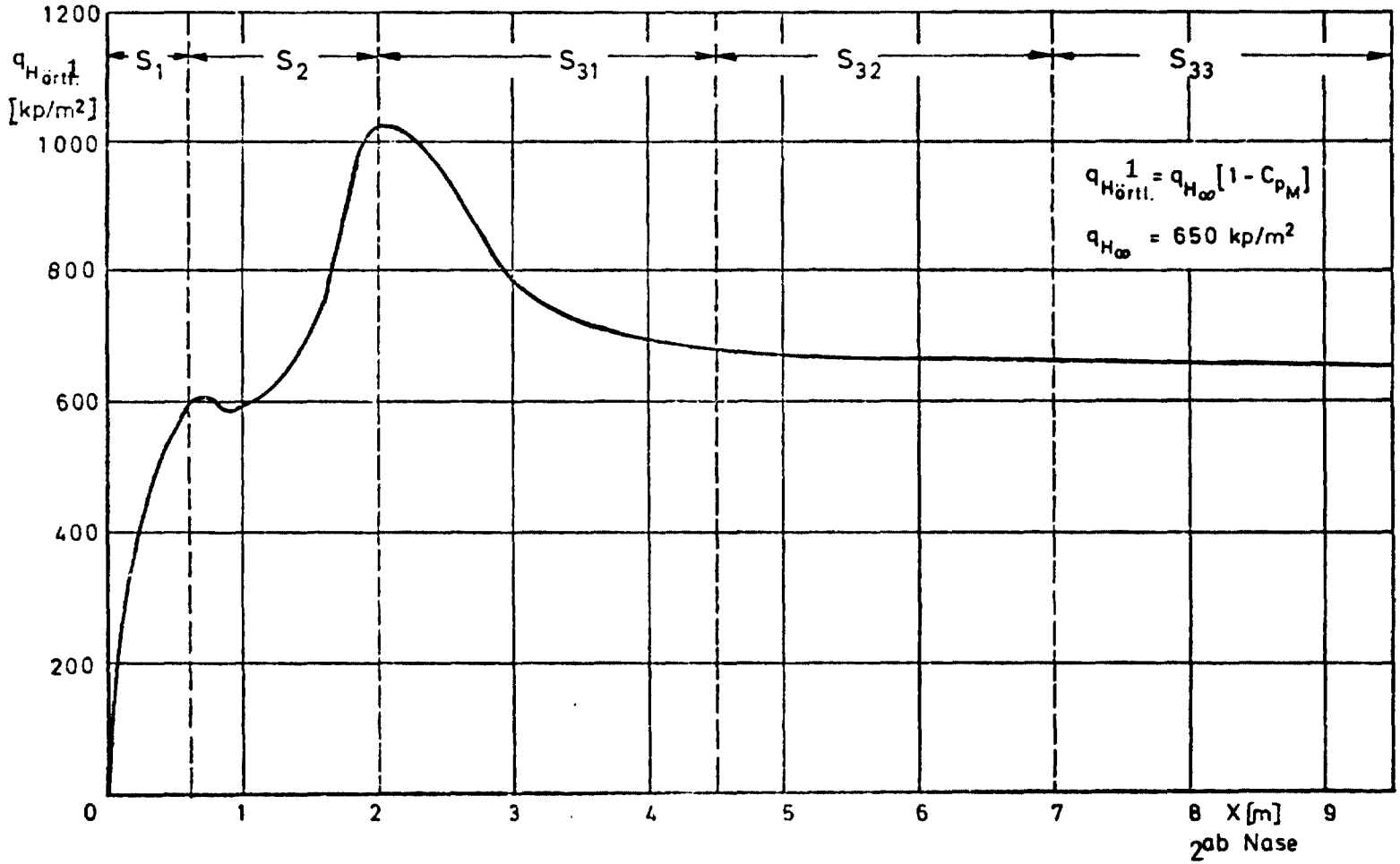

Diagram 1: Stagnation Pressure at the Fuselage Side (from Model Measurements $\alpha \approx 0°$)

Key: 1-local 2-from nose

Figure 1. Main Dimensions

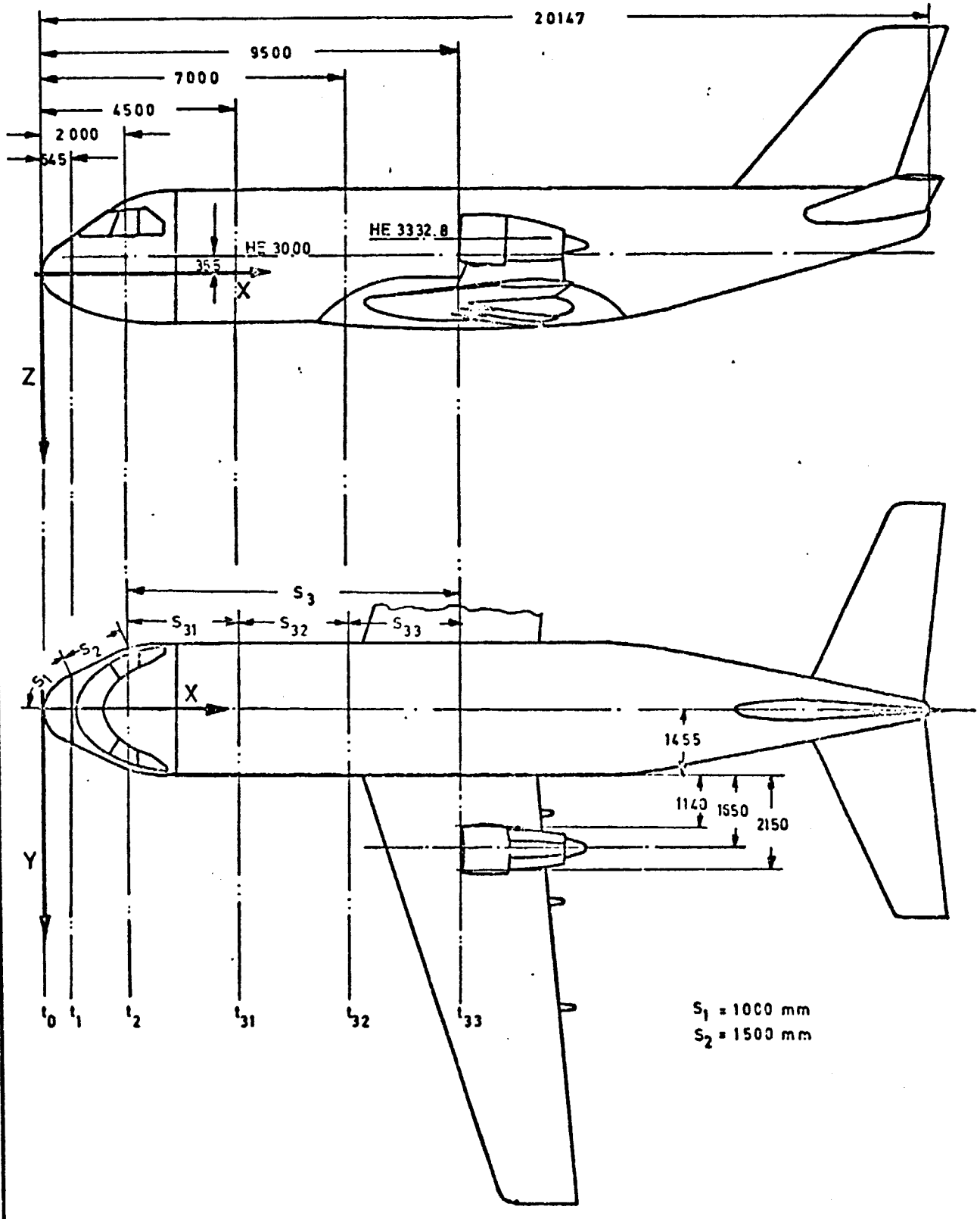

Fig. 2: Flight Path in Case 1

Key: 1-case 1; 2-ice cube with 3-edge length 4-resistance 5-flight path

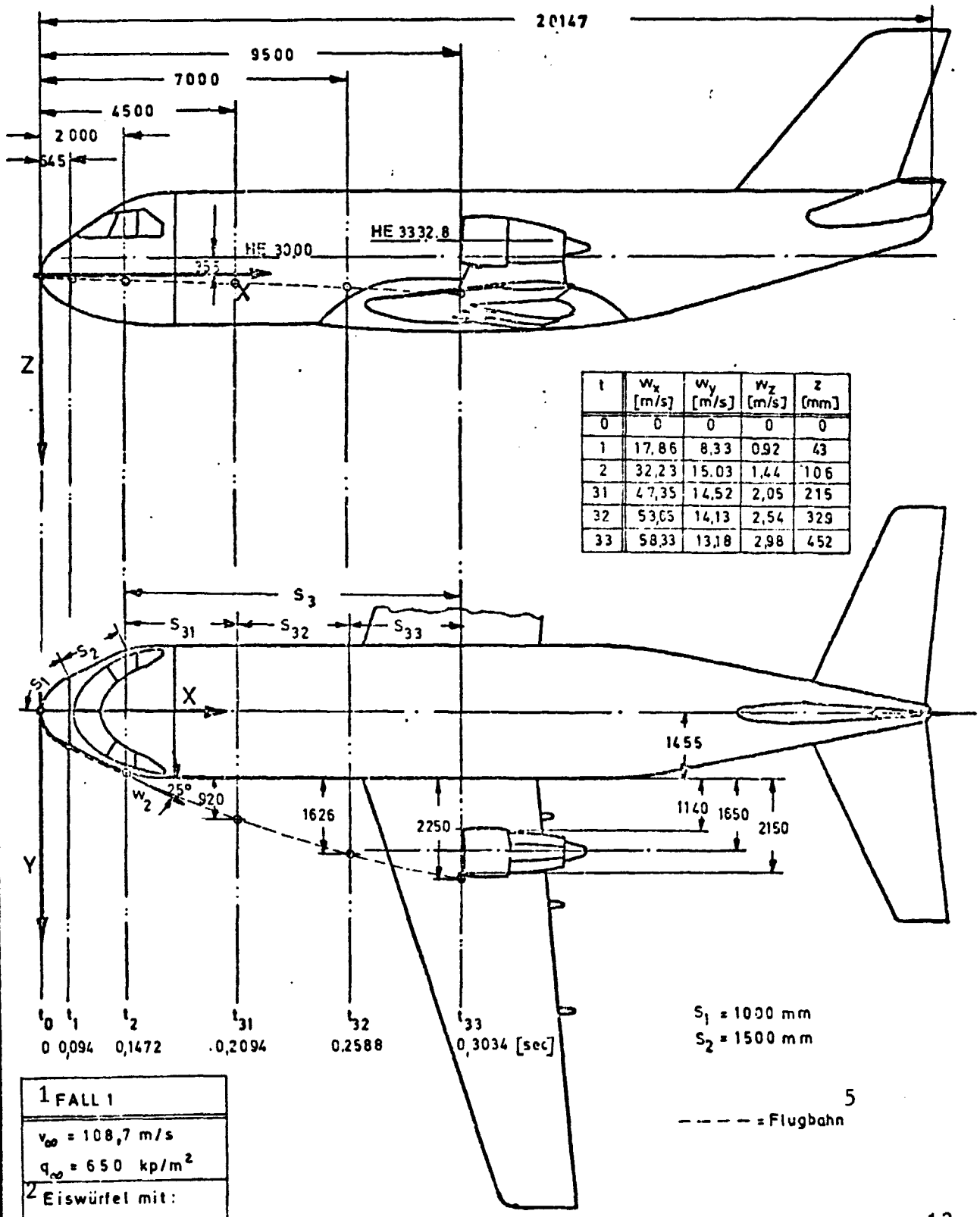

t	w_x [m/s]	w_y [m/s]	w_z [m/s]	z [mm]
0	0	0	0	0
1	17,86	8,33	0,92	43
2	32,23	15,03	1,44	106
31	47,35	14,52	2,05	215
32	53,05	14,13	2,54	329
33	58,33	13,18	2,98	452

1 FALL 1
v_∞ = 108,7 m/s
q_∞ = 650 kp/m²
2 Eiswürfel mit:
3 • Kantenlänge 10mm
4 • Widerstand C_w = 0,7

Fig. 3. Flight Path in Case 2

Key: 1-case 2; 2-ice cube with 3-edge length 4-resistance 5-flight path

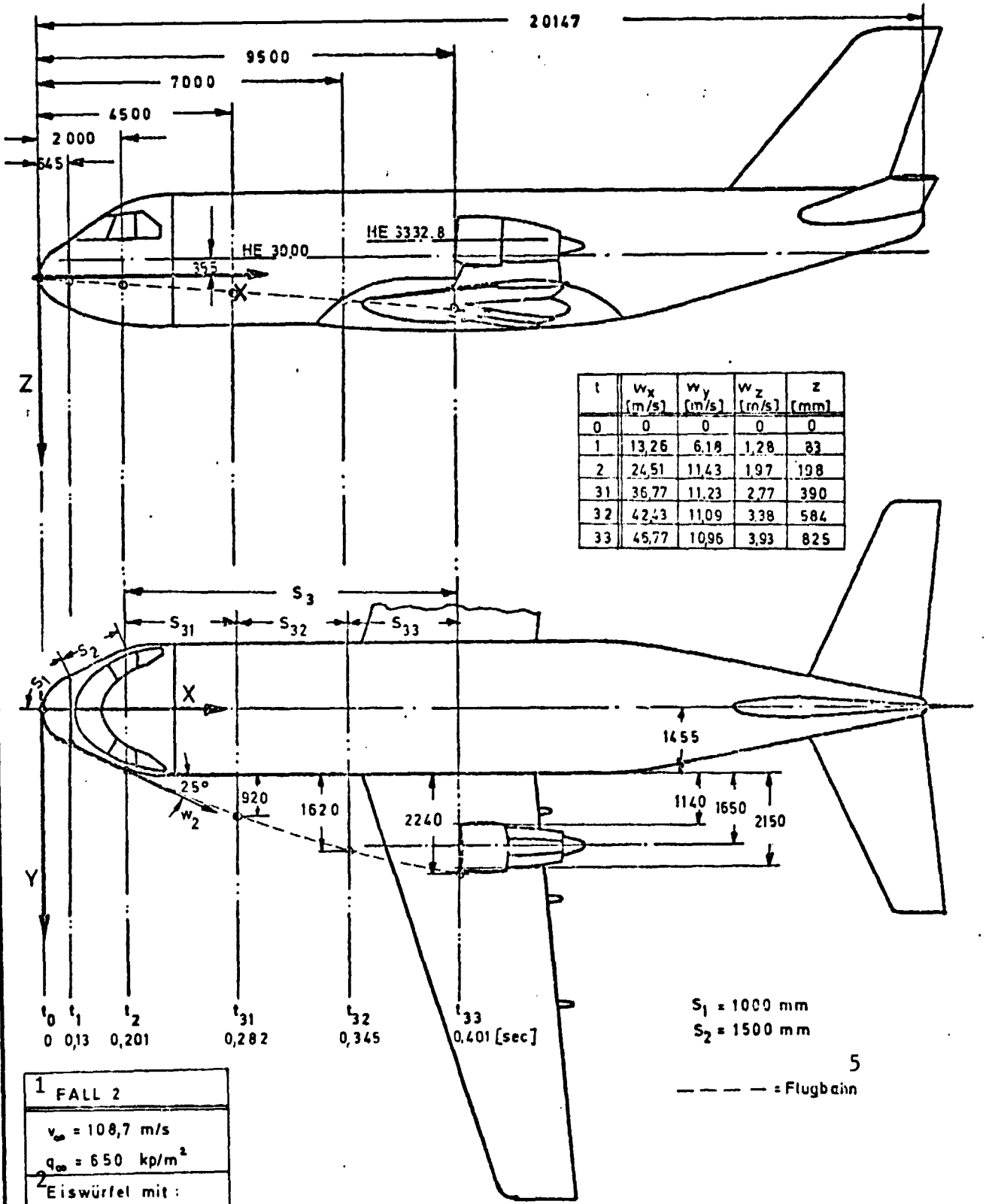

t	w_x [m/s]	w_y [m/s]	w_z [m/s]	z [mm]
0	0	0	0	0
1	13,26	6,18	1,28	83
2	24,51	11,43	1,97	198
31	36,77	11,23	2,77	390
32	42,43	11,09	3,38	584
33	46,77	10,96	3,93	825

1 FALL 2

v_∞ = 108,7 m/s

q_∞ = 650 kp/m²

2 Eiswürfel mit:

3 Kantenlänge 20 mm

4 Widerstand C_W = 0,7

Fig. 4. Flight Path in Case 3

Key: 1-case 3; 2-ice cube with 3-edge length 4-resistance 5-flight path

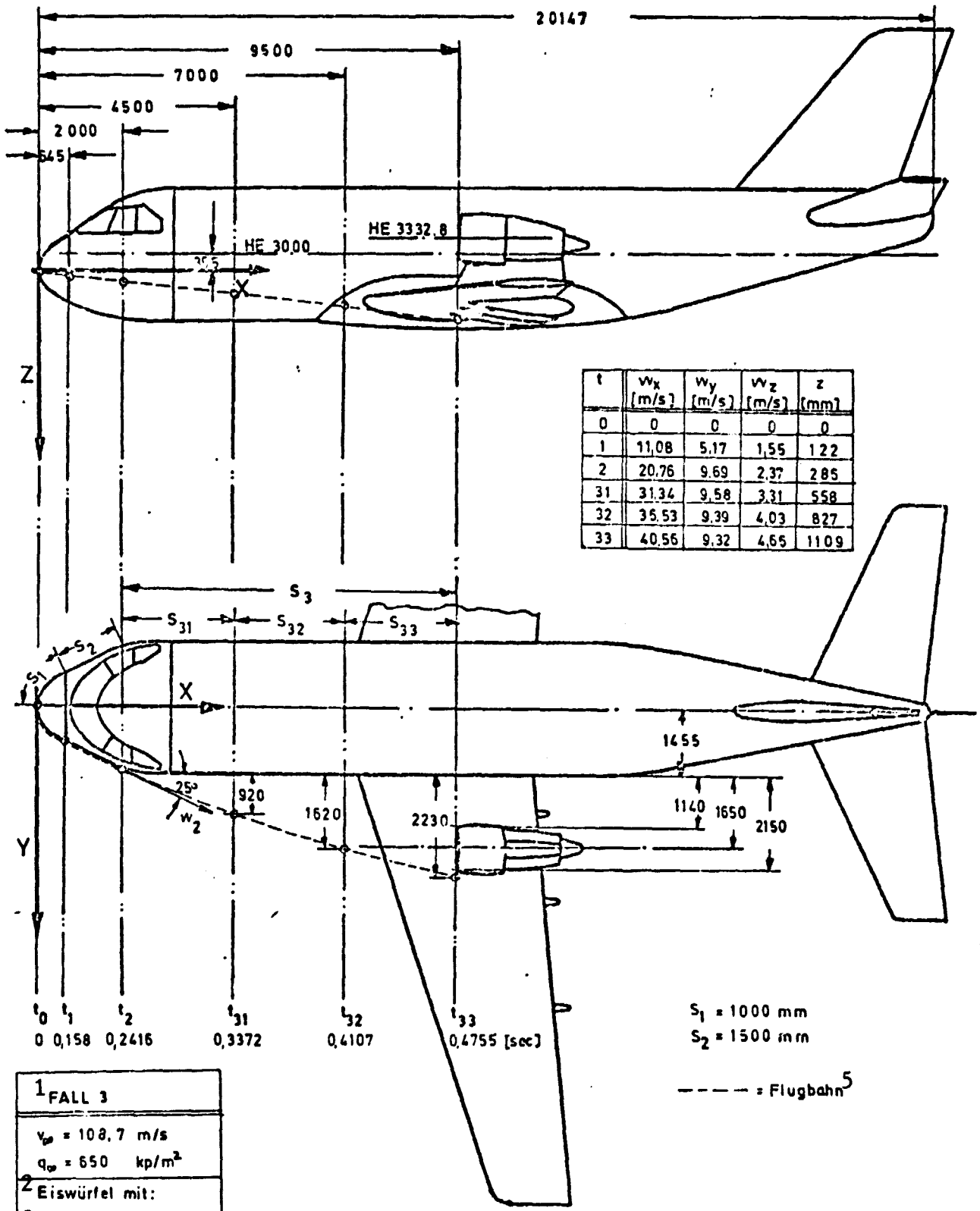

t	w_x [m/s]	w_y [m/s]	w_z [m/s]	z [mm]
0	0	0	0	0
1	11,08	5,17	1,55	122
2	20,76	9,69	2,37	285
31	31,34	9,58	3,31	558
32	35,53	9,39	4,03	827
33	40,56	9,32	4,65	1109

1 FALL 3

v_∞ = 108,7 m/s

q_∞ = 650 kp/m²

2 Eiswürfel mit:

3 • Kantenlänge 30 mm

4 • Widerstand C_W = 0,7

Fig. 5: Flight Path in Case 4

Key: 1-case 4; 2-ice cube with 3-edge length 4-resistance
5-flight path

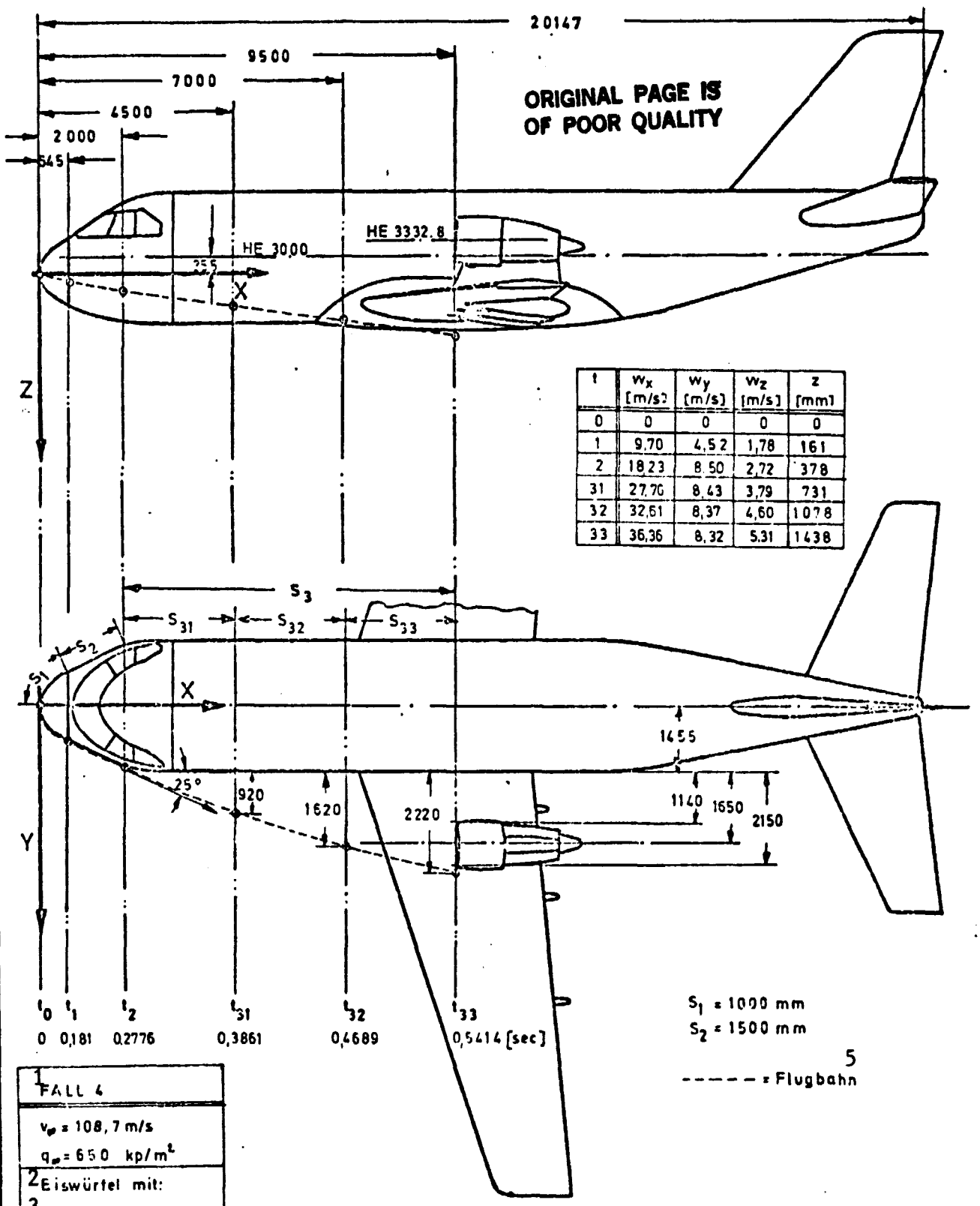

ORIGINAL PAGE IS
OF POOR QUALITY

t	w_x [m/s]	w_y [m/s]	w_z [m/s]	z [mm]
0	0	0	0	0
1	9,70	4,52	1,78	161
2	18,23	8,50	2,72	378
31	27,70	8,43	3,79	731
32	32,61	8,37	4,60	1078
33	36,36	8,32	5,31	1438

1 FALL 4

v_∞ = 108,7 m/s

q_∞ = 650 kp/m²

2 Eiswürfel mit:

3. Kantenlänge 40 mm

4. Widerstand c_w = 0,7

Fig. 6: Influence of Quadrant Angle of Departure on the Flight Path

Key: 1-case 1 and 1*; 2-ice cube with 3-edge length 4-resistance 5-path 6-angle between v_2 and x-axis

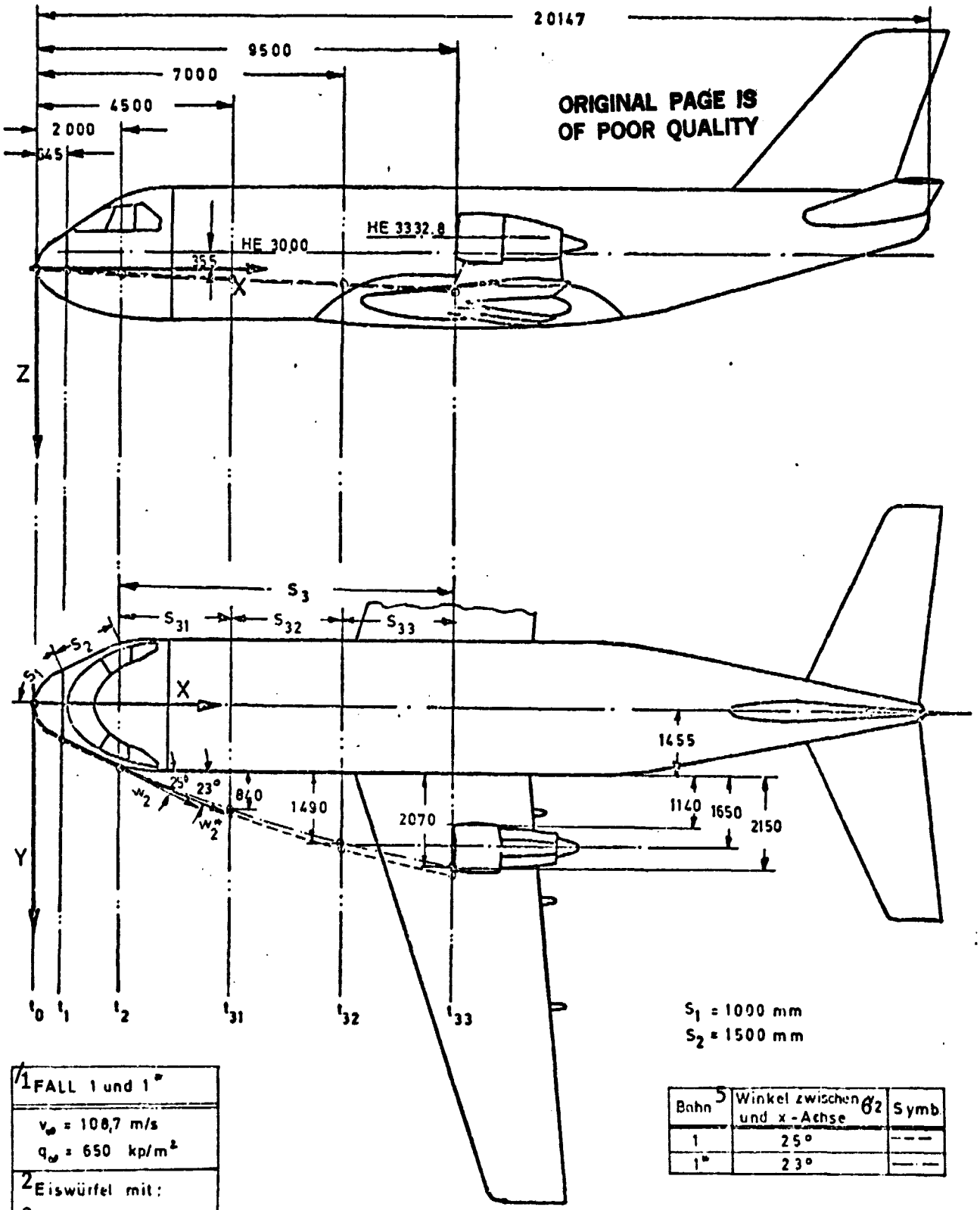

1 FALL 1 und 1*
v_∞ = 108,7 m/s q_∞ = 650 kp/m²
2 Eiswürfel mit: 3. Kantenlänge 10 mm 4. Widerstand C_w=0,7

Bahn 5	Winkel zwischen v_2 und x-Achse 6	Symb
1	25°	– – –
1*	23°	— —

Fig. 7: Influence of Angle of Incidence on the Flight Path in Case 1

Key: 1-case 1; 2-ice cube with 3-edge length 4-resistance

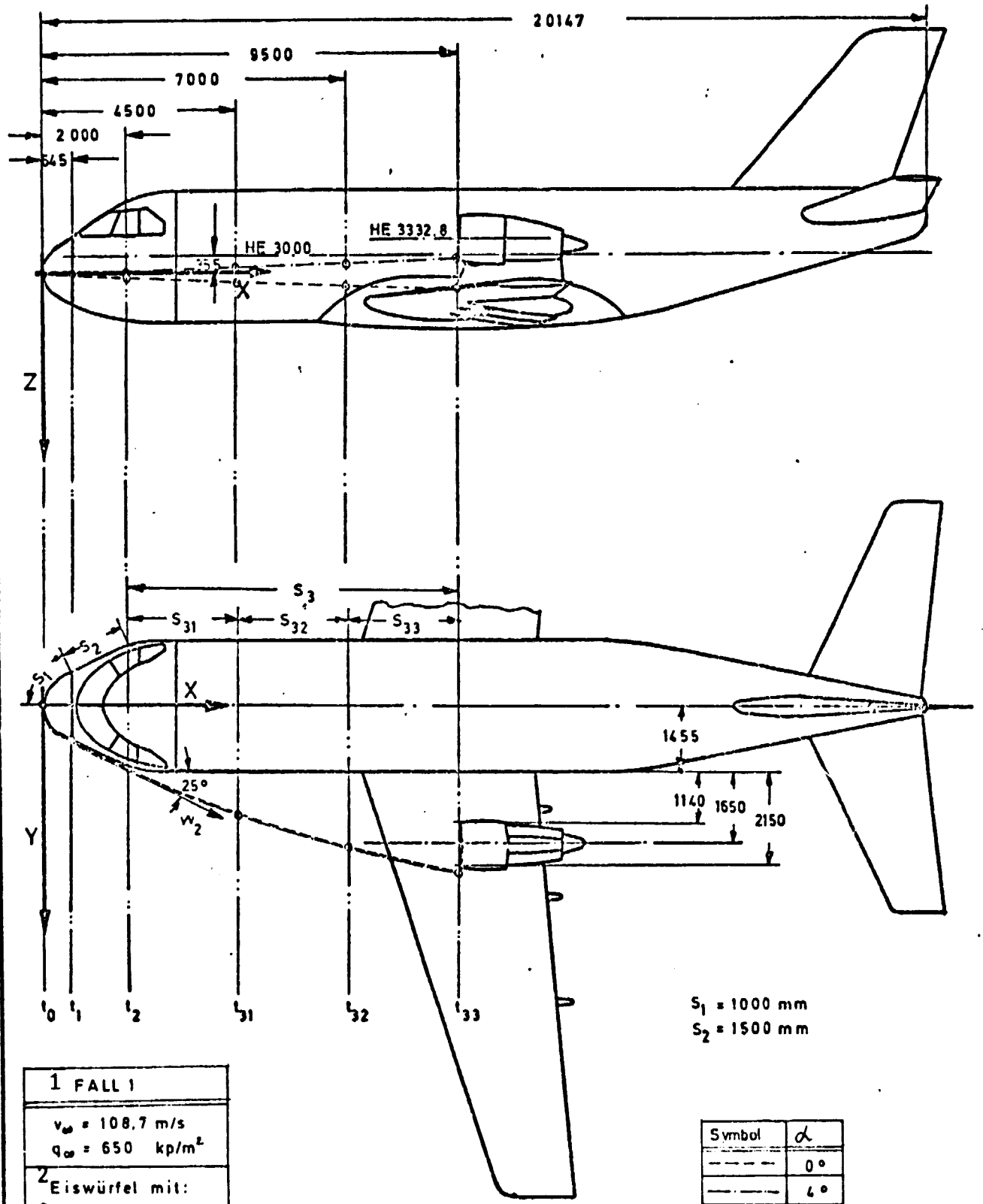

REPORT Ef 586, Part 2

Subject: Similarity Laws as Preparation for Wind Tunnel Tests with Ice Separation

Summary: Within the frame of the aerodynamic investigations on the VFW 614--ice separation--tests were performed in the VFW Fokker Eiffel wind tunnel on a scale model. In order to have valuable results on the flight paths of separated ice particles on the large scale version, the similarity mechanics for model tests had to be derived and taken into account.

In part 2 of this report, the model laws and their application to a specific flight state are presented.

Bearbeitet / Prepared	Geprüft / Checked	Gebilligt / Approved	Anerkannt / Acknowledged

Verteiler / Copy to:	Neuausgabe / Re-issue: Datum / Date:	Bem. / Remarks:
	And.-Ausg. / Revision: Seite / Page: Datum / Date:	
Datum/Date: Ausg./Rev.No.:		Anz. der Seiten: 8 Numb. of Pages:

Contents

1. Introduction

When applying scale models to a problem, basically not all similarity requirements can be fulfilled. One must then decide on the essentials and formulate the applicable simulation laws. In particular in the description of free-flight processes in a wind tunnel--like spiral diving, load dropping or ice break-off--the dynamic sequence must be taken into account. Other--usually important--criteria, as described for instance, by the Mach or Reynolds coefficient, may become unimportant.

2. Definitions

L Useful lift $= C_L \cdot \varrho_L \cdot v^2 \cdot l^2$

C_L Coefficient of aerodynamic lift

ϱ Density of the free-flying body (here: Ice)

ϱ_L Density of the surrounding medium (here: Air)

T Mass inertia $= m \cdot b = \varrho \cdot l^3 \cdot b$

b Linear acceleration (general)

g Acceleration of gravity (as special case of b)

m Mass of free-flying body (here: Ice) $= \varrho \cdot l^3$

G Gravity of the free-flying body (here: Ice) $= \varrho \cdot l^3 \cdot g$

l Characteristic length of aircraft and free-flying body

v Relative speed, body--medium

λ Model scale $= \frac{l_{FS}}{l_m}$

$\frac{\sigma}{\varrho}$ Body-density ratio $= \frac{\varrho_m}{\varrho_{FS}}$

Relative air density $\frac{\varrho_{L_{FS}}}{\varrho_{L_m}} = \frac{\varrho_H}{\varrho_o}$

With the indices:

m Model

FS Aircraft (full scale)

o ISA, H = 0

H ISA, H > 0 (flight altitude)

3. Simulation Laws

The forces acting on the ice particle are:

- o The aerodynamic force L
- o The mass inertia T, and
- o Gravity G.

Thus, the first similarity law must be:

$$\frac{L_m}{T_m} = \frac{L_{FS}}{T_{FS}} \qquad (1)$$

In addition, the limiting requirement must be taken into account that the occurring longitudinal accelerations b have to be derived in the same ratio as the earth's acceleration. That is:

$$\frac{G_m}{T_m} = \frac{G_{FS}}{T_{FS}} \qquad (2)$$

Thus, the Froude law must be fulfilled

$$\frac{v_m^2}{g_m \cdot l_m} = \frac{v_{FS}^2}{g_{FS} \cdot l_{FS}} \qquad (3)$$

At the flight altitudes under consideration(H ~ 2000 m)we may set:

$$g_m = g_{FS} \qquad (4)$$

Thus, (3) is simplified to:

$$\frac{v_m^2}{v_{FS}^2} = \frac{l_m}{l_{FS}} = \frac{1}{\lambda} \qquad (3a)$$

From eq. (1) results the following relation:

$$\frac{C_{L_m} \cdot \varrho_{L_m} \cdot v_m^2 \cdot l_m^2}{\varrho_m \cdot b_m \cdot l_m^3} = \frac{C_{L_{FS}} \cdot \varrho_{L_{FS}} \cdot v_{FS}^2 \cdot l_{FS}^2}{\varrho_{FS} \cdot b_{FS} \cdot l_{FS}^3} \qquad (1a)$$

and from this, with $C_{L_m} \approx C_{L_{FS}}$:

$$\frac{v_m^2}{v_{FS}^2} = \frac{\bar{\varrho} \cdot \sigma}{\lambda} \qquad (1b)$$

For complete simulation of the required criteria, we must have:

$$\bar{\varrho} \cdot \sigma = 1 \qquad (5)$$

as a comparison of (1b) with (3a) shows.

In the applicaiton of the model, this means:

1. The rel. air density $\bar{\varrho}$ is usually determined from the flight altitude H and the density in the wind tunnel
2. The scale factor λ is usually specified from the stock of suitable models, thus:
3. The velocity ratio is already determined and
4. The density of the model particle: (ϱ_m)

is specified from: $\varrho_m = \sigma \cdot \varrho_{FS} = \frac{\varrho_{FS}}{\bar{\varrho}}$

For body and path quantities, there results the following scales for "complete simulation":

Quantity radio FS/m	Scale
Length	λ
Velocity	$\sqrt{\lambda}$
Time	$\sqrt{\lambda}$
Longitudinal acceleration	[1]
Body density	$\bar{\varrho}$
Air density	$\bar{\varrho}$
Stagnation pressure	$\lambda \cdot \bar{\varrho}$
Aerodynamic lift, Mass inertial forces, Gravitational forces	$\lambda^3 \cdot \bar{\varrho}$

Sometimes, the scale requirement for the model body density

$$\varrho_m = \frac{\varrho_{FS}}{\bar{\varrho}} \qquad (6)$$

cannot be followed exactly. Reasons for this can be both in the procurement of material, and in the photographic limits of path recording.

In such compulsory deviations from requirement (6), only the simulation law (1b)

$$\lambda \cdot \frac{v_m^2}{v_{FS}^2} = \bar{\varrho} \cdot \sigma$$

is fulfilled; the simulation is "incomplete". Nonetheless, the achieved model results can be valid, as for instance:

$$0{,}5 \leq \bar{\varrho} \cdot \sigma \leq 2{,}0$$

is valid. As proof, we can use a velocity variation. The scale table contains the "incomplete" simulation of the following picture:

Quantity ratio FS/m	Scale
Length	λ
Velocity	$\sqrt{\frac{\lambda}{\varrho \cdot \sigma}}$
Time	$\sqrt{\lambda \cdot \varrho \cdot \sigma}$
Longitudinal acceleration	$\frac{1}{\varrho \cdot \sigma}$
Body density	$\frac{1}{\sigma}$
Air density	$\frac{\varrho}{\sigma}$
Stagnation pressure	$\frac{\varrho}{\sigma}$
Aerodynamic lift Mass inertial forces Gravitational forces	$\frac{\lambda^3}{\sigma}$

4. Applied Example

$$v_{\infty_{FS}} = 200 \text{ kn} = 102{,}9 \text{ m/s}$$

$$H = 1{,}8 \text{ km} \Rightarrow \bar{\varrho} = \frac{L_{FS}}{L_m} = 0{,}8382$$

$$\frac{l_{FS}}{l_m} = \lambda = 15$$

The best-possible model for the model ice would be:

$$\varrho_m = \frac{\varrho_{ice}}{\bar{\varrho}}$$

$$= \frac{0{,}918}{9{,}81} \cdot \frac{1}{0{,}8382} = 0{,}112 \quad \frac{kp\,s^2}{m^4}$$

or

$$\gamma_m = \varrho_m \cdot g = 1{,}1 \quad \frac{g}{cm^3}$$

We have available:

Wood: $\gamma_m \sim 0{,}4 \quad \frac{g}{cm^3}$

Acrylic glass: $\gamma_m \sim 1{,}19 \quad \frac{g}{cm^3}$

Teflon: $\gamma_m \sim 2{,}22 \quad \frac{g}{cm^3}$

The weight requirement is best met by acrylic glass, whereas--as pretests showed--teflon is best for the path simulation.

In order to have a representative statement on the path profile of a separated ice particle on the full-scale item, comparison tests with different weight materials are to be performed on the model.

REPORT Ef 586, Part 3

Subject: Wind Tunnel Investigations on Ice Separation from the VFW 614
Measurement Report of Measurements WX 75-13.

Summary: Tests on ice separation were conducted on the flight testing model of the VFW 614 on a 1:15 scale in the VFW Fokker wind tunnel with the goal of determining the possible origin of ice particles which can get into the engine inlet.

As possible ice separation locations, there were three primary candidates:

1. Radome region
2. Cockpit region
3. Leading wing edge in the engine region

(Summary continued on next page)

Bearbeitet / Prepared	Geprüft / Checked	Gebilligt / Approved	Anerkannt / Acknowledged
May			B. Schmidt

Verteiler Herren		Neuausgabe / Re-issue: Datum / Date:	Bem. / Remarks:
Schäffler	E		
Kathen	Eo 2		
Issel	Ev 12		
Rummel/Held	Ek 244		
Krenz	Ef 1		
Ewald	Ef 2		
Franz	Ef 21	Änd.-Ausg. / Revision: Seite / Page: Datum / Date:	
Anders	Ef 22		
Burgsmüller	Ef 22		
May	Ef 21		
Datum/Date: 12.1.77			Anz. der Seiten: 50
Ausg./Rev.No.:			Numb. of Pages:

Summary (continued)

I. Measured Results

For the investigated flight condition $v_\infty \approx 200$ kts; $\alpha = 0 \ldots 4°$; $\beta = 0°$; $\eta_K = -6°$; $H \approx 6000$ ft, on the basis of the measured results we can say:

1. Radome Region

In the upper region of the radome ice pack, any separating particles follow flight paths--at angles of incidence of $0 \leq \alpha \leq 4°$ --which lead near the engines in the x, z-plane. In the x, y-plane this path curve depends on the angle of sideslip β. If $\beta = 0$, the flight paths run outside the engine plane, but for smaller sideslip angles, they could endanger an engine, if

① $-5° \leq \beta < 0°$ for the Bb engine

② $0° < \beta \leq 5°$ for the Stb-engine

Since during the test flight, only sideslip angles of $\beta \approx 0°$ were used, a damage to the engines by "Radome ice separation" is not very likely for the studied state.

2. Cockpit Region

The flight paths of the ice pacticles breaking off from the cockpit region were higher than the engine inlets in the measurements, so that possible engine damage is very unlikely.

3. Leading wing edge in the engine region

Ice particles breaking off the leading wing edge can endanger the engines. The conducted measurements showed that ice separation in the area of ca. 0.5% I (y) on the pressure side up to ca. 1% I(y) on the suction side is particularly critical for the studied state.

II. Note

It must be expressly pointed out that all measured data and statements of this report relate exclusively to the simulated ice separation on the studied flight stand. The selected size of "ice

particles and their separation positions were specified and thus under some circumstances, can differ from reality.

Contents

1. Introduction

After a "deicing test flight" of the VFW 614, damage was found on the fan blades of the two engines.

In connection with the investigations to explain the origin of the damage, in the period from 11/28 to 12/9/75, measurements were conducted in the VFW Fokker wind tunnel with the 1:15 flight-testing model.

Since damage to the engines is supposed to be caused by loosened ice particles, the goal of these measurements was to determine the flight profiles of these particles.

The following regions were considered possible separation positions:

1. Radome
2. Cockpit
3. Leading wing edge in the engine area.

2. Measurement Set-Up

2.1 Description of the Model

The measurements on trajectory description were conducted with the available 614 Flight testing model (MP 69-14, scale 1:15). The model (without HLW) installed in the measurement lane was modified to simulate loosening ice particles as follows:

a) Fuselage nose

Installation of openings in the radome and cockpit area for the insertion of a device for ejecting the simulated "ice".

b) Wing

Insertion of two magnetic rails with an electromagnet in the leading wind edge.

c) Whole Model

Model painted black to reduce light reflection.

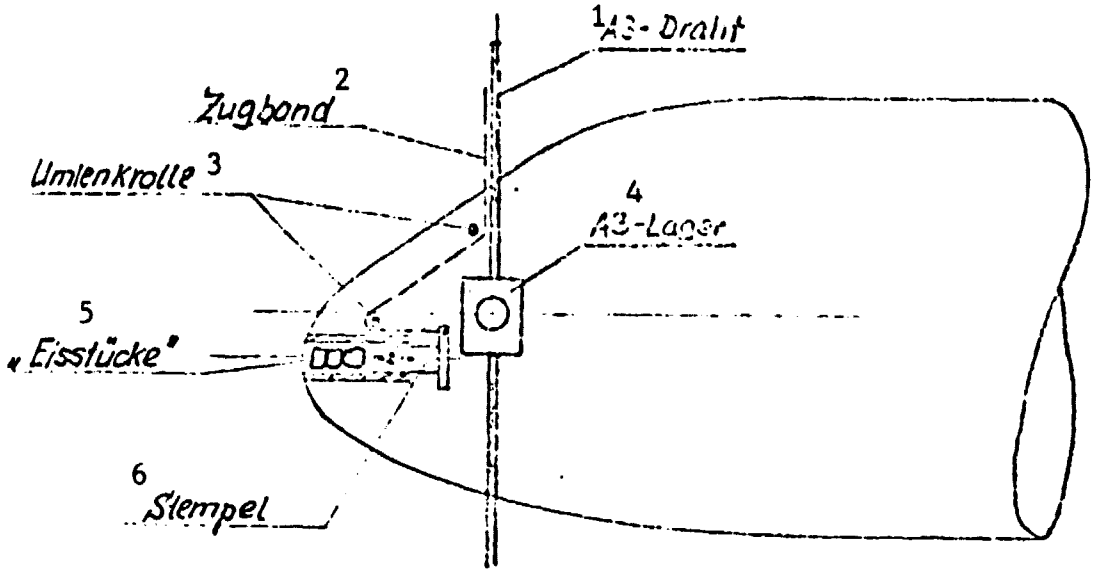

Key: 1-A3 wire; 2-tie rod 3-guide pulley 4-A3-bearing 5-"ice particles" 6-stamp

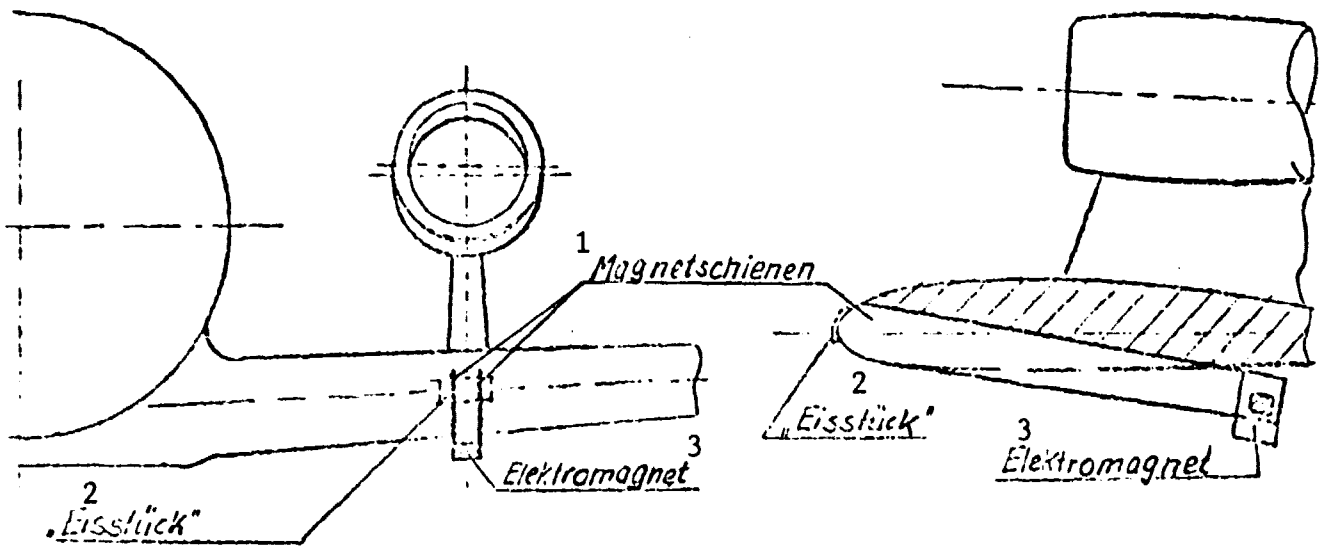

Key: 1-magnetic rails 2-"ice particles" 3-electromagnet

2.2 Ice Build-up on the Fuselage

As potential ice separation positions in the forward fuselage area, two regions came into consideration:

1. Radome
2. Cockpit

2.2.1 Radome Region

Since no information is available on the ice build-up during the test flight, the position and size must be specified on the basis of earlier "ice build-ups".

The radome build-up of 50 to 60 mm diameter established for the model measurements, was simulated by irregular plastic applications of 0-3 mm to better simulate the actual nose air circulation.

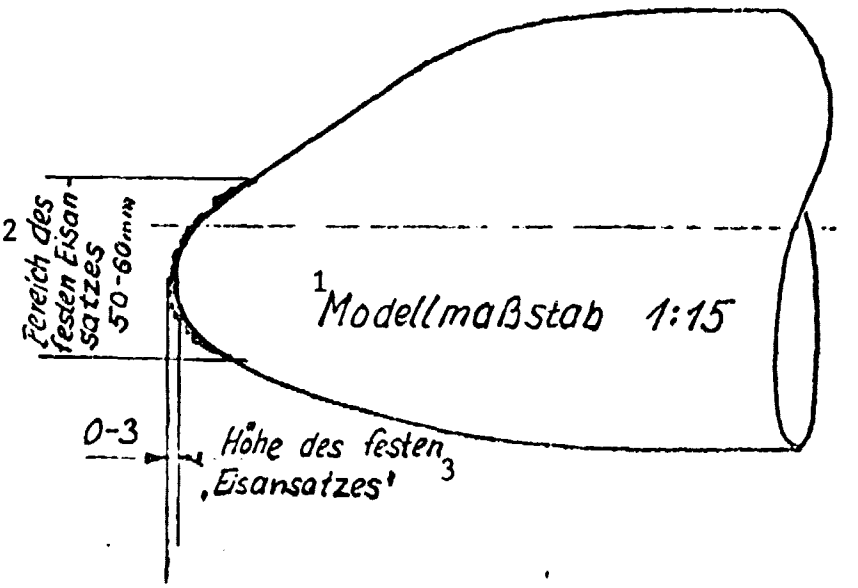

Key: 1-model scale 1:15; 2-region of solid ice build-up 3-height of solid ice build-up

The separation of ice particles could be simulated at two radome positions with the installed ejection device.

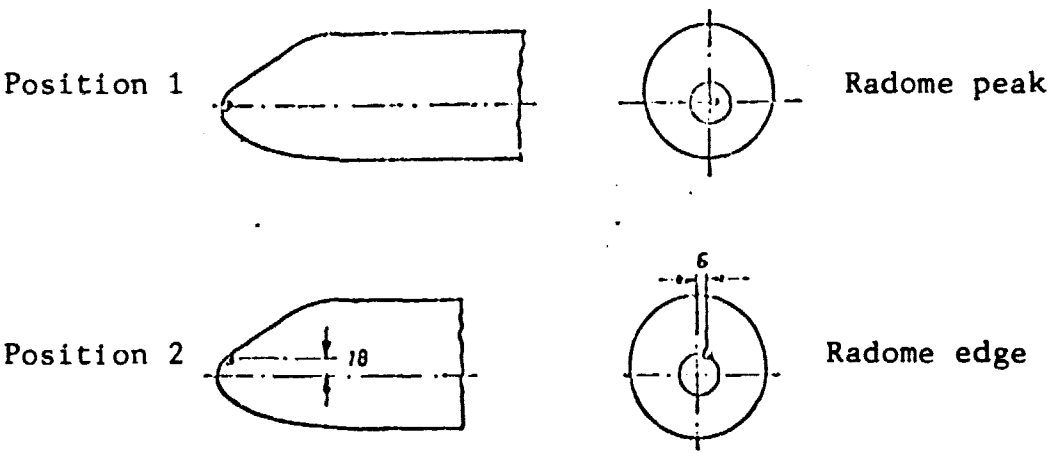

2.2.2 Cockpit Region

According to statements by VFW 614 pilots, during the "ice flights", larger ice blocks formed on the cockpit windshield wipers, which sometimes also broke off. In the model test, this was simulated by the ejection device installed at position 4.

Position 4

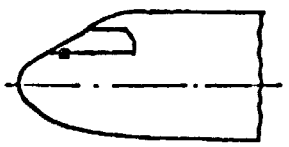

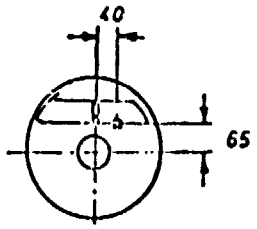

Windshield wiper area

2.3 Ice Build-up on the Wing

In normal flight operations, the formation of ice on the leading wing edge should be prevented by the deicing system installed in the VFW 614. To implement the test program, this system was not switched on immediately in the "damaged flight" in spite of the prevailing icing conditions.

According to the pilot, a rapidly increasing ice charge formed on the leading wing edge, which began to disintegrate after switching on the deicing system, with the frequent separation of ice particles.

But more precise statements about the size, location and nature of these ice particles could not be given, so that a larger number of possible separation positions had to be investigated for the model tests.

The sketch below shows the 4 selected separation positions.

Eispositionen am Flügel

Ice Positions on the Wing

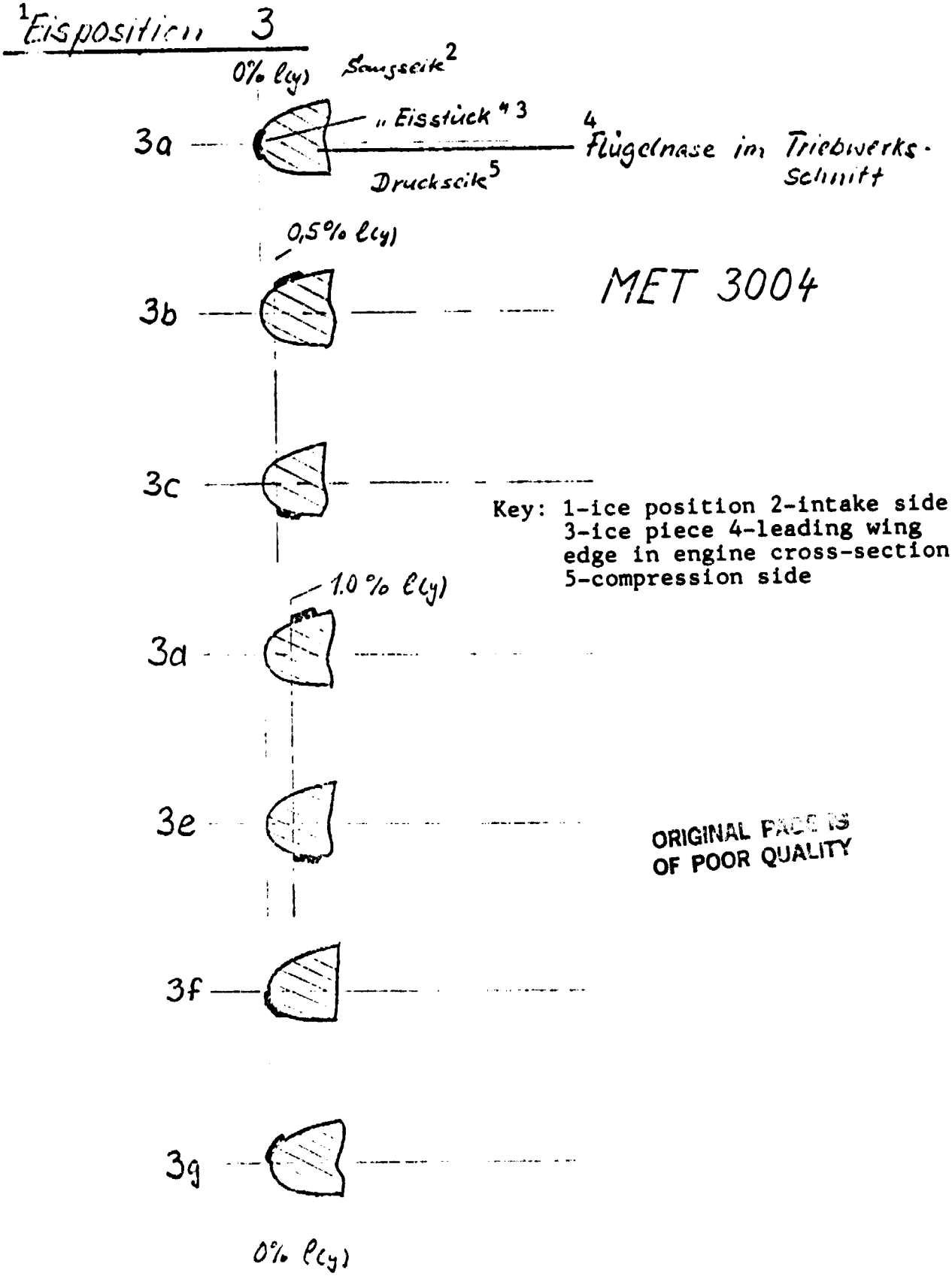

Key: 1-ice position 2-intake side 3-ice piece 4-leading wing edge in engine cross-section 5-compression side

Datum/Date:		Seite/Page: 10/.
Ausg./Rev.No.:		Dok. Nr.:

VFW 2084-1

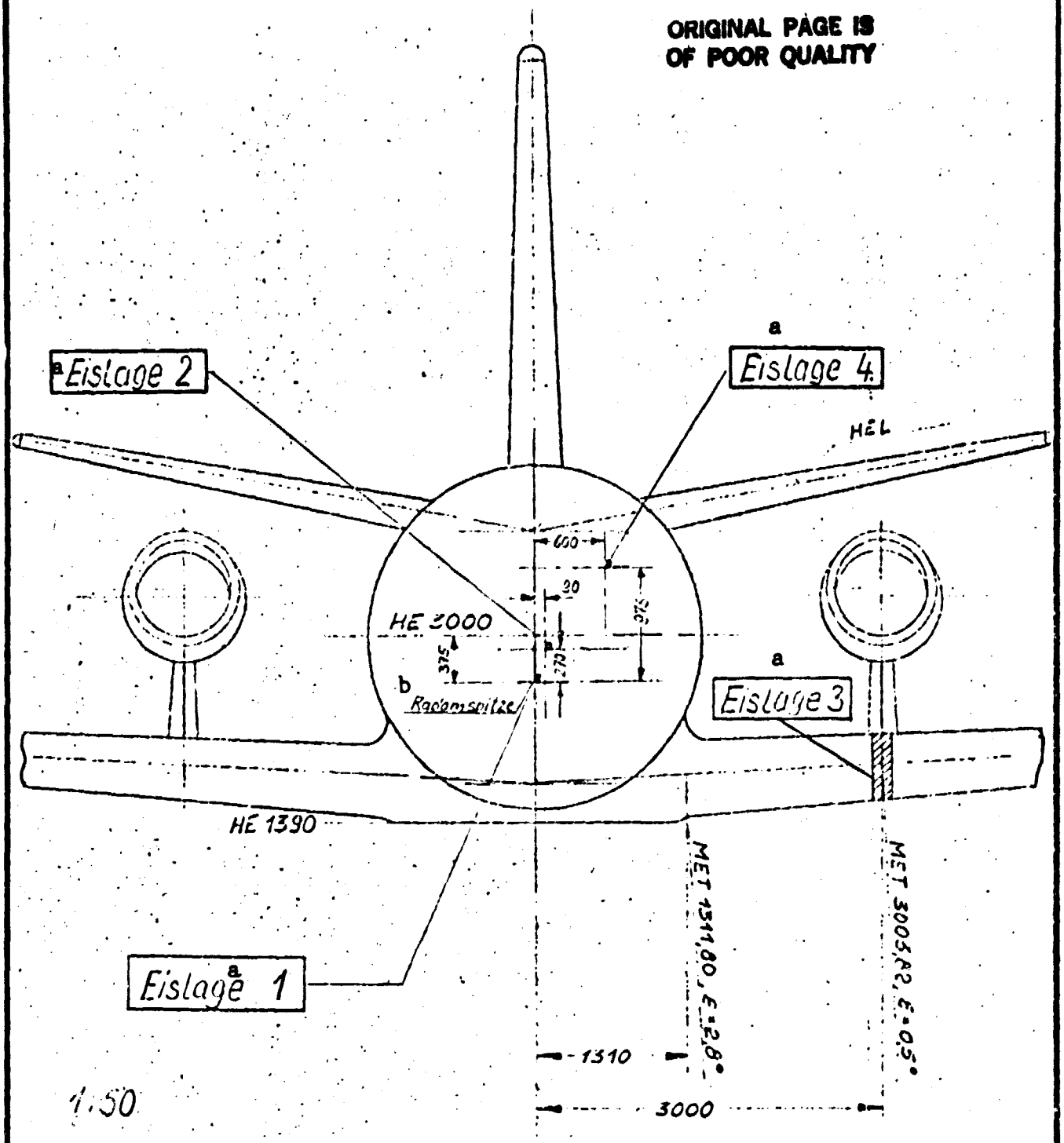

Key: 1-ice position 2-radome peak

11/.

2.4 Simulation of Ice Particles

2.4.1 Radome and Cockpit

At the radome (positions 1 and 2) and cockpit (position 4), the breaking "ice particles" are represented by small blocks and are pressed out from the described positions from the fuselage nose by means of the sketched device.

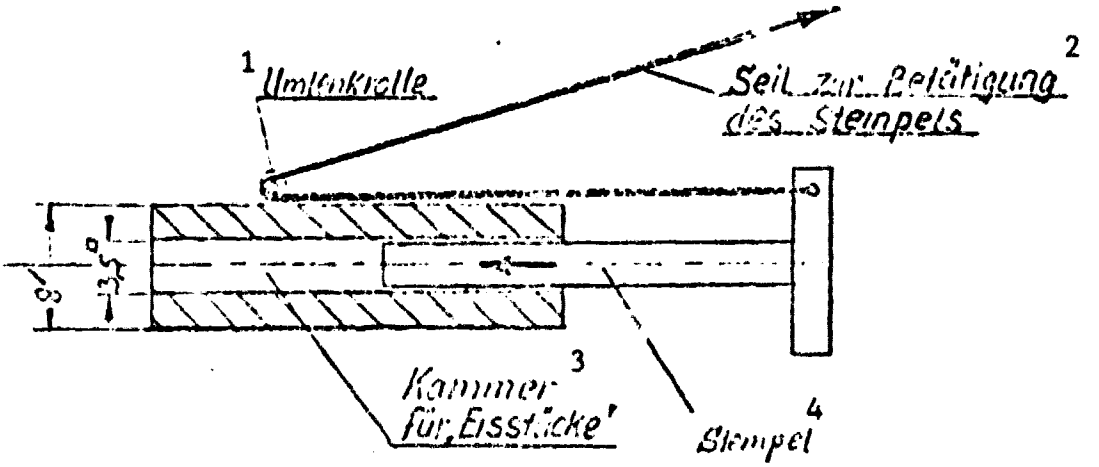

Key: 1-guide pulley 2-rope for operation of the stamp 3-chamber for "ice particles" 4-stamp

The different-sized blocks had the following dimensions

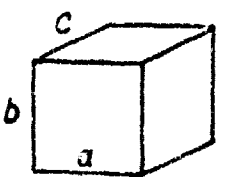

$2 \leq a \leq 3$ mm

$2 \leq b \leq 3$ mm

$2 \leq c \leq 5$ mm

As discussed in part 2 of this report: "Similarity laws as a Preparation of Wind Tunnel Tests with Ice Separation", for the model tests, a material of $\gamma \approx 1,1$ gr/cm^3 should have been used.

For reasons of photographic flight-path recording however, the main fraction of measurements was conducted with "ice particles" of white teflon. Pretests had shown that only very bright particles reflect sufficient light for a photographic recording of flight paths. The sole suitable material available was teflon with $\gamma \approx 2,2$ gr/cm^3.

In addition, some tests were performed with acrylic glass $\gamma \approx 1,2$ gr/... and wood $\gamma \approx 0,5$ gr/cm^3 in order to get a more representative idea of the path profile in the full-scale design.

2.4.2 Leading Wing Edge

The simulated wing ice particles consisted of a thin, magnetic piece of sheet metal which was held in place by an electromagnet until its release from the leading wing edge.

By gluing on various materials to these sheet-metal strips, a total of 14 types with differing density and volume were prepared. Samples of these "ice particles" are found in the measurement documentation in the wind tunnel.

Ice type	Weight	Volume	Spec. Weight
	p	cm^3	p/cm^3
X1	≈ 0,15	≈ 0,033	≈ 4,5
X2	≈ 0,30	≈ 0,066	≈ 4,5
X3	≈ 0,05	≈ 0,033	≈ 1,5
X4	≈ 0,10	≈ 0,066	≈ 1,5
X5	≈ 0,05	≈ 0,027	≈ 1,9
X6	≈ 0,10	≈ 0,050	≈ 2,0
X7	≈ 0,20	≈ 0,027	≈ 7,5
X8	≈ 0,30	≈ 0,043	≈ 7,0
X9	≈ 0,45	≈ 0,073	≈ 6,2
X10	≈ 0,55	≈ 0,099	≈ 5,5
X11	≈ 0,05	≈ 0,168	≈ 0,3
X12	≈ 0,10	≈ 0,336	≈ 0,3
X13	≈ 0,15	≈ 0,112	≈ 1,3
X14	≈ 0,15	≈ 0,320	≈ 0,5

2.5 Measurement Set-up in the Wind Tunnel

Of the various possibilities for flight-path determination of simulated ice particles, a photographic representation was a low-cost method. During its flight, the "ice particle" was illuminated

several times on its way from the break-off point to the engine plane by a stroboscope, and all these "flash photographs" were recorded by a camera.

To reduce the disturbing light reflection from the model and tunnel walls, they were blackened and the measurement-lane windows were darkened.

The "ice ejection device" at the fuselage nose and the electromagnet for the "wind ice attachment" could be operated from outside the measurement lane.

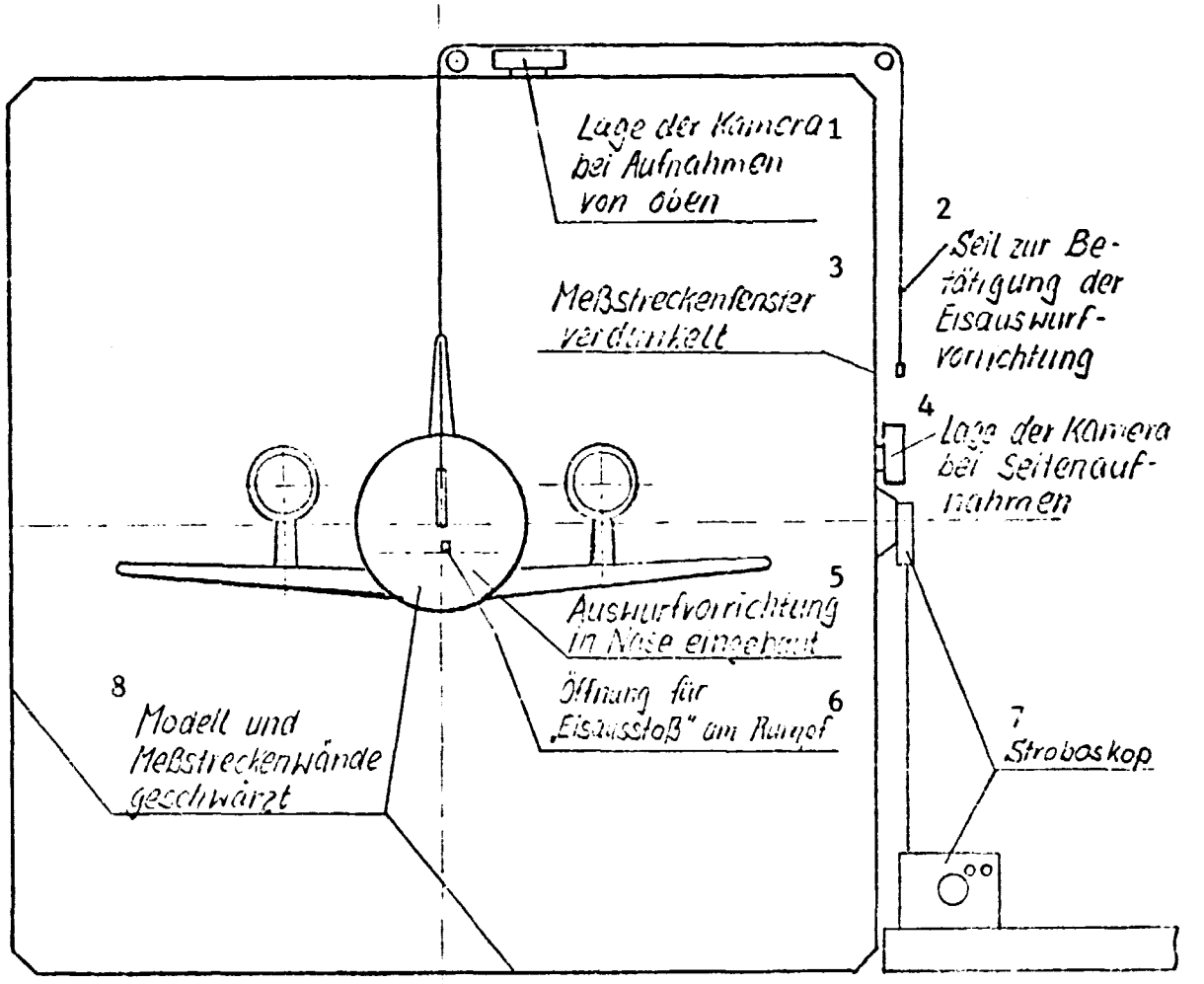

Measurement Set-up for "Ice Separation" from the Radome and Cockpit

Key: 1-location of camera for photography from above 2-rope to operate the ice ejection device 3-darkened measurement-lane window 4-location of camera for photography from the side 5-ejection device installed into nose 6-opening for "ice ejection" from fuselage 7-stroboscope 8-model and tunnel walls blackened.

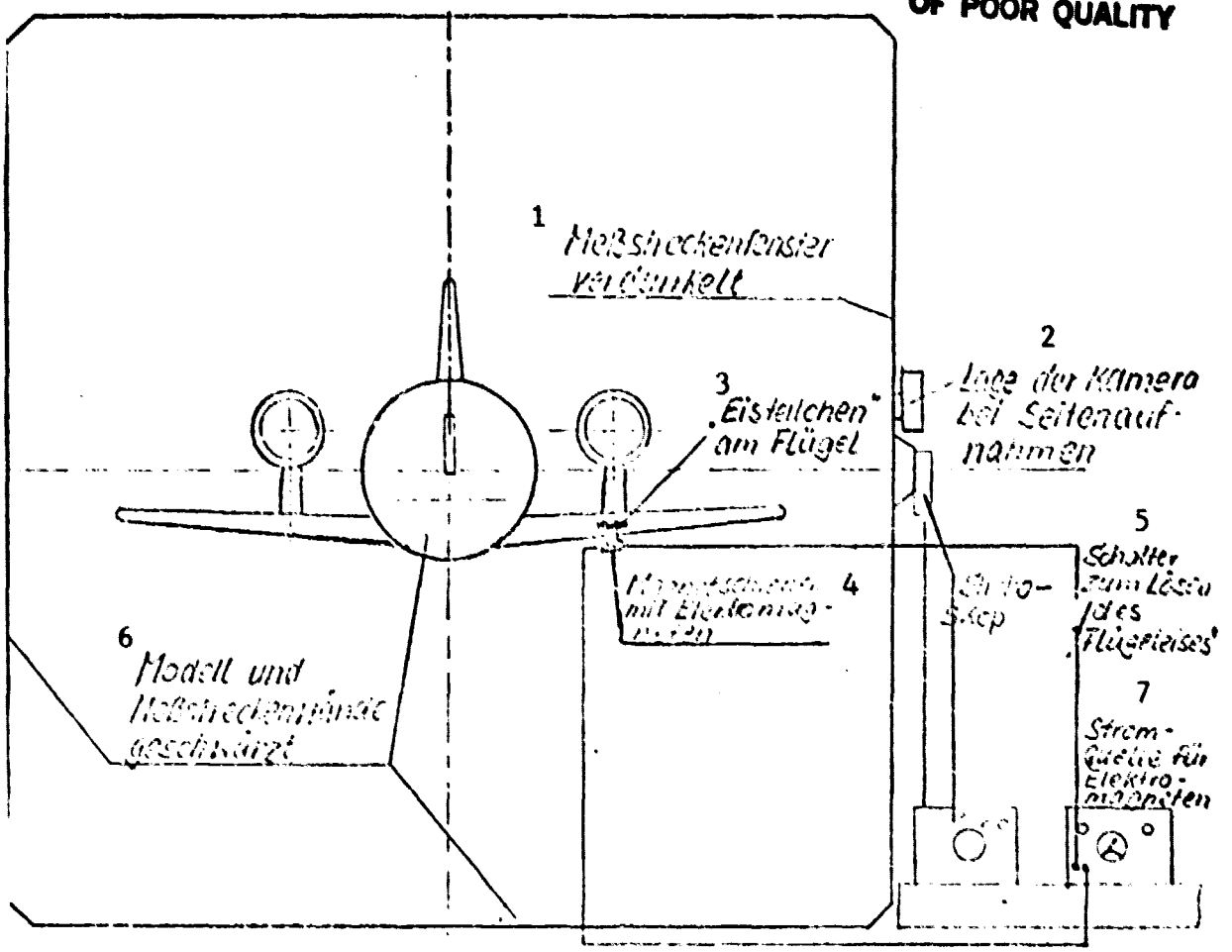

Measurement Set-up for "Ice Separation" from the Wing

Key: 1-measurement-lane window darkened 2-location of camera for photography from the side 3-"ice particles" on the wing 4-magnetic rails with electromagnet 5-switch to loosen the "wing ice" 6-model and measurement-lane walls blackened 7-power source for electromagnets

3. Implementation of Testing

3.1 General Information

Specified test parameters, besides the supposed ice separation positions of radome, cockpit and leading wing edge, for the flight state when engine damage occurred, were:

$$V_\infty \approx 200 \text{ kts}$$

$$\alpha_M \approx 0 \ldots 4^\circ$$

$$\beta_M \approx 0^\circ$$

$$\eta_M \approx -6^\circ$$

$$\text{Altitude} \approx 6000 \text{ ft}$$

The model measurement was performed with the 1:15 VFW 614 flight testing model MP 69-14, without HLW; without modified leading wing edge; with engine gondola; $\eta_K = -6°$.

The similarity conditions to be met as completely as possible in each model test were determined in this case primarily by the inertial forces $\sim \rho \cdot v^2$ and the gravity $\sim \rho \cdot g \cdot l$ or by their ratio of the Froude coefficient:

$$Fr = \sqrt{\frac{\rho \cdot v^2}{\rho \cdot g \cdot l}} = \sqrt{\frac{v^2}{g \cdot l}}$$

(see also part 1 of this report).

Besides the selected test speed of $v_\infty \approx 26$ m/s ($\hat{=}$ $q_\infty \approx 42$ kp/m^2) to reinforce the applicability to the full-scale design, measurements with $v_\infty \approx 37$ m/s ($\hat{=}$ $q_\infty \approx 85$ kp/m^2) or $v_\infty = 40$ m/s ($\hat{=}$ q_∞ 100 kp/m^2) were conducted for several configurations.

For the same reason, besides teflon with $\gamma \approx 2{,}2$ p/cm^3, two other materials were selected for ice simulation at radome and cockpit:

Wood with $\gamma \approx 0{,}5$ p/cm^3 and
Plexiglass $\gamma \approx 1{,}2$ p/cm^3.

For the wing ice simulation, a total of 12 "ice particles" of differing size and density were used (section 2.4.2).

3.2 Determination of Approach Paths at the Radome and Cockpit

As already described in sec. 2.4.1, the best qualitative flight path photographs were obtained when using teflon blocks to simulate the "ice".

For each test, the ejection device sketched on page 38 was filled with 5 or 6 such blocks. After setting the test parameters (q_∞, α, β) the stamp was moved forward slowly by the rope leading out of the measuring lane. Thus, the "ice particles" were pressed in sequence to the model surface and carried off by the tunnel air flow. During its flight from the fuselage nose down to the engine

plane, each particle's position was determined by stroboscopic photography. From the particle spacing between two photographs and the flash-photography sequence, the average particle speeds can be determined.

The path profile in the x, z-plane and x, y-plane was determined by the two photography positions:

1. From the side
2. From above.

In the preliminary tests it turned out that at a stroboscope flash frequency of f = 100 Hz, the majority of path positions could be adequately determined. The entire measuring program was thus performed at this flash frequency.

3.3 Determination of Approach Paths at the Wing

In contrast to the radome and cockpit ice separation, "magnetic ice particles" were held securely to the leading wing edge by an electromagnet. After switching off this electromagnet, the "ice particles" were carried off by the wind tunnel flow and their paths were photographed.

Due to the low light reflection of the "ice particles", the image quality achieved in the radome and cockpit tests could not be duplicated. The relatively black electromagnet and the reduction in magnetic force by the provisional installation of magnetic rails caused the separation of "ice particles" to occur often before triggering the camera. To prevent frequent repeat measurements, an additional observation record was kept.

3.4 Measuring Program

For reasons of cost and time, the selection of test parameters was limited to the data reported in the test flight. The following wind tunnel logs provide an overview of the measuring program.

WIND TUNNEL LOG
Model position: 3
Month/year: 12/75

Project: WX 75-13, 614 Ice Separation
Model: 614 Flight Testing Model 1:15
without HLW; no modified leading wing edge

a Tag	b Meßreihe	Parameter							c Fotoaufn.		Lesung	d Bemerkungen	Diagr.
		v_{co} [kts]	α_{nL} [°]	β_{nL} [°]	γ_K [°]	Expo-sition	Eis-tag	Eis-typ	von	Filmnr.			
2.	4258	42	c/418 10/12/14	0	-6	Radom	1	Y1	x oben	1,2,4			
"	4259	42 (156)	418/10 12/14	+5	"	"	"	"	"	"			
3.	4260	42	0/418 10/12/14	0	"	"	"	"	der i Seite	2,3			
"	4261	"	418/10 12/14	+5	"	"	"	"	"	3			
"	4262	"	0/2/ 4/6	0	"	"	2	"	i oben	5			
"	4263	"	"	+5	"	"	"	"	"	"			
"	4264	"	2/4	-5	"	"	"	"	"	"			
"	4265	"	"	"	"	"	"	"	der i Seite	6			
"	4266	42 (100)	0/4/2 6	0	"	"	"	"	"	"			
"	4267	42	"	+5	"	"	"	"	"	"			
4.	4268	"	4	0	"	k Flügel	3a-3g	X1, X2	"	7			
5.	4269	"	0/2/4	"	"	Cockpit	4	Y1	"	8			
"	4270	"	2/4	+5	"	"	"	"	"	"			
"	4271	"	"	-5	"	"	"	"	"	"			
"	4272	"	0,5/2 4/6	0/ +5	"	k Flügel	3a/ 3g	X1/ X2/X3	"	"			
"	4273	"	0/4	0	"	Cockpit	4	Y2	"	"			
"	4274	"	"	"	"	"	"	Y3	"	"			
6	4275	"	0/2/4	"	"	Radom	2	Y2	"	9			
"	4276	"	"	"	"	"	"	Y3	"	"			
"	4277	"	2/4	"	"	"	"	Y1	"	"			

Key: a-day b-series c-photo no. d-remarks e-ice position f-ice type
g-from h-film log i-above j-side k-wing l-see sketch and description in section 2

k Siehe Skizze und Beschreibung in Punkt 2 l

WIND TUNNEL LOG Project: WX 75-13, 614 Ice Separation
Model position: 3 Model: 614 Wing test model 1:15, no HLW; no modified
Month/year: 12/75 leading wing edge
Key: a-day b-series c-photo no. d-ice position d-ice type e-from
f-film log g-remarks h-side i-above j-wing

a Tag	b Meßreihe				Parameter									Lichtung	g Bemerkungen	Diagr.
					q_∞ [kp/m²]	α_M [°]	β_M [°]	γ_K [°]	Eisposition d	Eis-Farbe	Eis-Typ d	Foto-aufn. e	Filmprotokoll f			
6.	4	2	7	8	42	0/2/4	0	-6	Flügel i	3a / 3g	X10/X9 X8/X11	der Seite j	10			
8.	4	2	7	9	"	"	"	"	Radom	2	Y2	oben i	11			
"	4	2	8	0	"	0/4	"	"	"	"	Y3	"	"			
"	4	2	8	1	85/100	0	"	"	"	"	Y1	"	"			
"	4	2	8	2	"	"	"	"	"	"	"	der Seite j	"			
"	4	2	8	3	421/85	"	"	"	"	"	Y2	"	"			
"	4	2	8	4	"	0/2	"	"	Flügel i	3a / 3f	X7	"	11/12			
"	4	2	8	5	421/85/100	0	"	"	Cockpit	4	Y1	"	12			
"	4	2	8	6	"	"	"	"	"	"	Y2	"	"			
"	4	2	8	7	"	"	"	"	"	"	Y1	oben i	"			
"	4	2	8	8	"	"	"	"	"	"	Y2	"	"			

4. Test Results

4.1 General Information

Although an analysis of measured results by Ef2 was not included in the test authorization, the essential results will be described briefly.

Through the limitation of test parameters to data of the test flight, the measurements cannot give any extensive statement about the danger to engines from breaking ice particles. On the basis of the available results, it should be possible to estimate other flight paths, e.g. ice separation from the leading wing edge with extended flaps, likewise ice separation from other positions of the radome.

An overview of existing flight-path photographs of radome, cockpit and wind ice-separation is found on pages 46-54. For cost reasons, only two sets of flight profiles were produced, and one set was sent to Eo as the purchaser, whereas the second set remained in the VFW Fokker wind tunnel.

4.2 Ice Separation from the Fuselage

The existing flight path photographs were sorted by test parameters using the film log and assigned to various flight path classes (pages 46-50).

Next, the individual configurations were examined for their probability of hits in the engine and classified accordingly (pages 51-54).

Since the ice type Y3(plexiglass) with a spec. weight of $\gamma \approx 1,2\ gr/cm^3$ which comes closest to the spec. weight for the model test of $\gamma \approx 1,1\ gr/cm^3$, in the evaluation of the flight path photos of the different ice types, the following items must be taken into account:

a) The photos with ice type Y1 correspond approximately to the state of an approximately 4^o larger angle of incidence.

b) The photos with ice type Y2 correspond approximately to the state of an approximately 2° smaller angle of incidence.

Thus, for the examined ice separation positions from the fuselage there results the following probability of damage to the engine for the individual configurations:

Ice position	α [°]	β [°]	y_m [%]	Probability of danger to 3a-TW**	Stb-TW**
1	≤ 4	0	42... 100	1	1
	4... 8	|	|	1...2	1...2
	8... 10	|	|	2...3	2...3
	> 10	0	42.. 100	< 2	< 2
	≤ 4	-5	42... 100	1	1
	4... 8	|	|	2...3	1...2
	8.. 10	|	|	3...4	1...2
	> 10	-5	42... 100	< 3	1
	≤ 4	+5	42... 100	1	1
	4... 8	|	|	1.. 2	2...3
	8... 10	|	|	1.. 2	3...4
	> 10	+5	42... 100	1	< 3
2	≤ -4	0	42... 100	1	1
	-4... -2	|	|	2...3	2... 3
	-2... 0	|	|	3... 4	3... 4
	0... 2	|	|	3... 2	3... 2
	> 2	0	42... 100	< 2	< 2
	≤ -4	-5	42... 100	1	1
	-4... -2	|	|	2... 3	1.. 2
	-2... 0	|	|	3... 4	2
	0... 2	|	|	3... 2	2
	> 2	-5	42... 100	< 2	< 2
	≤ -4	5	42... 100	1	1
	-4... -2	|	|	1... 2	2.. 3
	-2... 0	|	|	2	3... 4
	0... 2	|	|	2	3... 2
	> 2	5	42... 100	< 2	< 2
4	≤ -6	-5/0/5	42... 100	≤ 2	≤ 2
	-6... -4	|	|	2...3	2...3
	-4... -2	|	|	3... 2	3... 2
	-2... 0	|	|	2 1	2...1
	> 0	-5/0/5	42... 100	1	1

**engine

*Probability of a hit: 0 none; 1 very low; 2 moderate; 3 high; 4 very large

Ice pos.	Ice type	MR	α	β	q_∞	The Flight Path of the Ice Particles Runs: in the x,z-plane				in the x,y-plane			Log
						near engine	over engine	under engine	under wing	near engine	outside engine	inside engine	Nr 02
/	/	/	°	°	$\frac{Kp}{m^2}$								
1	41	4258	4	0	42					X			02-1
		4260	4						X				24-06
		4260	8						X				24-10 12
		4258	10								X		24-1[illegible]
		4258								X			25-15
		4260	10						X				23-2[illegible] 26
		4258	12								X		23-1[illegible]
		4258								X	X		25-21
		4260				X		X					84-15
		4260							X				24-17
		4260	12					X	X				24-19
		4258	14					X					84-1
		4258				X							24-2
		4260	14	0							X		25-21 15
		4259	4	5	42						X		22-8
		4259			156						X		22-11
		4261	4		42				X				23-21 17
		4259	8								X		23-0[illegible]
		4261							X				84-23
		4261	8					X	X				84-24
1	41	4259	10	5	42						X		25-2

25- engine

Ice pos.	Ice type	MR	α	β	q_∞	The Flight Path of the Ice Particles runs: in the x,z-plane: near engine	over engine	under engine	under wing	in the x,y-plane: near engine	outside engine	inside engine	Log Nr 12
/	/	/	°	°	$\frac{Kp}{m^2}$								
1	41	4259	10	5	42						X		25-03
|	|	4261	|	|	|			X					24-28
|	|	4261	10	|	|			X	X				24-29
|	|	4259	12	|	|					X			23-05
|	|	4259	|	|	|					X			25-04
|	|	4261	|	|	|			X					24-30
|	|	4261	12	|	|	X							24-31
|	|	4259	14	|	|					X			25-10
|	|	4261	|	|	|		X						24-32
|	|	4261	|	5	|					X	X		24-35
|	|	4259	|	-5	|					X			25-13
1	41	4259	14	-5	42						X			25-14
2	41	4262	0	0	42							X		25-01
|	|	4281	|	|	85						X			27-10
|	|	4291	|	|	100					X	X			27-11
|	|	4265	|	|	42				X					27-02
|	|	4285	|	|	85			X						27-08
|	|	4295	0	|	100			X	X					27-09
|	|	4262	2	|	42						X			25-02
|	|	4266	|	|	42			X						27-05
2	41	4266	2	0	100	X	X	X							27-12

Bb- engine

Ice pos.	Ice type	MR	α	β	q_∞	The Flight Path of the Ice Particles Runs: in the x,z-plane				in the x,y-plane			Log
						near engine	over engine	under engine	under wing	near engine	outside engine	inside engine	
/	/	/	°	°	$\frac{Kp}{m^2}$								Nr 02
2	41	4262	4	0	100		X						87-10
		4266			42	X		X					87-2
		4265				X	X						87-9
		4262									X		86-44
		4262	4							X			86-91
		4262	6							X			86-114
		4262								X			86-124
		4265					X						87-15
		4266	6	0		X	X						87-13
		4263	0	5						X	X		86-134
		4267	0						X				87-18
		4263	2								X		86-134
		4267						X	X				87-21
		4267	2					X	X				87-23
		4263	4								X		86-284
		4267	4			X	X						87-25
		4263	6								X		86-294
		4267	6	5			X						87-224
		4264	2	-5								X	86-224
		4264								X			86-304
2	41	4265	2	-5	42			X	X				87-29

86- engine

Ice pos.	Ice type	MR	α	β	q_∞	The Flight Path of the Ice Particles Runs: in the x,z-plane				in the x,y-plane			Log Nr 02
/	/	/	°	°	$\frac{Kp}{m^2}$	near engine	over engine	under engine	under wing	near engine	outside engine	inside engine	
2	U1	4264	4	-5	42					X			86-[illegible]
		4264										X	86-[illegible]
		4265					X						87-30
	U1	4265	4	-5	42	X	X						87-34
	U2	4283	0	0	42		X						92-[illegible]
		4283			42		X						92-[illegible]
		4283	0		85		X						92-[illegible]
		4279	2		42					X			92-[illegible]
		4272								X			92-[illegible]
		4275	2				X						90-9
	42	4275	4				X						90-12
	43	4280	0								X		92-[illegible]
		4280									X		92-[illegible]
		4280									X		92-[illegible]
		4276					X						90-[illegible]
		4276	0			X	X	X					90-[illegible]
		4276	2				X						90-[illegible]
		4276	4				X						90-26
2	U3	4276	4	0	42	X	X						90-[illegible]

* Bb- engine

VEREINIGTE FLUGTECHNISCHE WERKE - FOKKER

C14 - Ice Separation from Fuselage
Evaluation of Flight Photos

Ice pos. /	Ice type /	α °	β °	q_∞ $\frac{kp}{m^2}$	Hit Probability for fin Bo-TW	Hit Probability for fin Sib-TW
2	42	2	0	42	2	2
	42	4			2	2
	43	0			2	2
		2			2	2
2	43	4	0	42	1-2	1-2
4	41	0	0	42-100	2-3	2-3
		2	5	42	2	2
		4	5		2	2
		2	-5		2	2
	41	4	-5		2	2
	42	0	0	42-100	2	2
	42	4		42	1	1
	43	0			2	2
4	43	4	0	42	1	1

TW=engine

*Hit probability: 0 none; 1 very low; 2 medium; 3 great; 4 very great

LMSA

Ice pos.	Ice type	MR	α	β	c_{ap}	The Flight Path of the Ice Particles Runs: in the x,z-plane				in the x,y-plane			Log
						near engine	over engine	under engine	under wing	near engine	outside engine	inside engine	
/	/	/	°	°	$\frac{Kp}{m^2}$								Nr 02
4	U1	4287	0	0	42					X	X		93-04
		4285				X							93-05
		4285			42	X		X					93-06
		4287			85					X	X		93-23
		4283			100					X			93-24
		4285			85		X						93-14
		4285	0	0	100		X						93-15
		4277	2	5	42	X							93-9
		4279	4	5		X							93-10
		4271	2	-5			X						93-17
	U1	4271	4	-5			X						93-18
	U2	4283	0	0	42							X	93-34
		4288			85							X	93-35
		4288			100					X		X	93-37
		4273			42		X						93-28
		4283			85		X						93-29
		4283	0		100		X						93-27
	U2	4272	4		42		X						93-27
	U3	4274	0				X						93-26
4	U3	4274	4	0	42		X						93-25

ORIGINAL PAGE IS OF POOR QUALITY

Ice Separation from Fuselage, Evaluation of Path Photos

E5- engine x

FLUGTECHNISCHE WERKE - FOKKER

GW - Ice Separation from Fuselage
Evaluation of Flight Photos

ice pos.	ice type	α	β	q_∞	Hit Probability for				
/	/	°	°	$\frac{kp}{m^2}$	Rü-TW	Stü-TW			
1	y1	≤ 4	0	42	0	0			
		8			1	1			
		10			2	2			
		12			2	2			
		14			2-3	2-3			
		> 14	0		< 3	< 3			
		≤ 4	5		0	0			
		8			1	1			
		10			1	2			
		12			2	3			
		14			2	4			
		> 14	5		< 2	< 4			
		≤ 4	-5		0	0			
		8			1	1			
		10			2	1			
		12			3	2			
		14			4	2			
1	y1	> 14	-5	42	< 4	< 2			
2	y1	≤ 0	0	42	1	1			
		0		85/100	2	2			
		2		42	2	2			
		2		100	3-4	3-4			
		4		42	3	3			
		4		100	2	2			
		6	0	42	2-3	2-3			
		0	5		1	1			
		2			1	2-3			
		4			2	3-4			
		6	5		2	2-3			
		2	-5		2-3	1			
	y1	4	-5		3-4	2			
	y2	0	0	42	2	2			
2	y2	0	0	85	2	2			

TW=engine

ORIGINAL PAGE IS OF POOR QUALITY

* Hit probability: 0 none; 1 very low; 2 medium; 3 great; 4 very great

VFW 77

FLUGTECHNISCHE WERKE - FOKKER K

577 - Ice Separation from Fuselage

Ice pos.	Ice type	α °	β °	$\frac{p_\infty}{kp/m^2}$	Hit Probability for / Port fin: BB-TW m X,Z-plane	BB-TW m X,y-plane	Stb.-TW m X,Z-plane	Stb.-TW m X,y-plane	
1	41	4	0	42	0	2	0	2	
		8			1	2	1	2	
		10			2	2	2	2	
		12			3	2	3	2	
		14	0		4	2	4	2	
		4		42	0	1	0	3	
		4		156	0	1	0	3	
		8		42	1	1	1	3	
		10			2	1	2	3	
		12			3	1	3	3	
		14	5		4	1	4	3	
		4	-5		0	3	0	1	
		8			1	3	1	1	
		10			2	3	2	1	
		12			3	3	3	1	
1	41	14	-5	42	4	3	4	1	
2	41	0	0	42	0	2	0	2	
		0		85	2	2	2	2	
		0		100	2	3	2	3	
		2		42	2	2	2	2	
		2		100	3	3	3	3	
		4		42	3	2	3	2	
		4		100	2	2	2	2	
		6	0	42	2	3	2	3	
		0	5		0	2	0	2	
		2			2	1	2	3	
		4			3	1	3	3	
		6	5		2	1	2	3	
		2	-5		2	3	2	1	
	41	4	-5		3	3	3	1	
	42	0	0	42	2	2	2	2	
		0		85	2	2	2	2	
?	42	?	0	42	?	?	?	?	

TW=engine

* Hit probability: 0 none; 1 very low; 2 medium; 3 great; 4 very great

VEREINIGTE FLUGTECHNISCHE WERKE - FOKKER

WX 75-13

C14 - Ice Separation from Fuselage

Blatt

ice pos.	ice type	α	β	q_∞	Hit Probability for: Bb - TW in X,Z-plane	Bb - TW in X,y-plane	Stb. - TW in X,Z-plane	Vert fin TW in X,y-plane	
/	/	°	°	kp/m^2					
2	42	4	0	42	1	3	1	3	
	43	0			3	2	3	2	
		2			2	2	2	2	
2	43	4	0	42	1	2	1	2	
4	41	0	0	42	3	2	3	2	
				85	2	3	2	3	
		0	0	100	2	3	2	3	
		2	5	42	3	2	2	3	
		4	5		3	2	2	3	
		2	-5		2	3	3	2	
	41	4	-5		2	3	3	2	
	42	0	0	42	2	2	2	2	
				85	2	2	2	2	
		0		100	2	3	2	3	
	42	4		42	1	2	1	2	
	43	0			2	2	2	2	
4	43	4	0	42	1	2	1	2	

TW=engine

31/.

* Hit probability: 0 none; 1 very low; 2 medium; 3 great; 4 very great

30/.

In summary, it was found that for all three release positions, similar flight paths resulted for differing angles of incidence:

1 Eistyp	2 Eislage 1	2 Eislage 2	2 Eislage 4
y1	$\alpha = 10...12° \hat{=}$	$\alpha = 0...2$	∴
y1	$\alpha = 12...14° \hat{=}$	$\alpha = 2...4° \hat{=}$	$\alpha = -2...0$
y2	∴	$\alpha \approx -2° \hat{=}$	$\alpha \approx 0°$
y3	∴	$\alpha \approx 2° \hat{=}$	$\alpha \approx 4°$

Key: 1-ice type 2-ice position

The different test bodies had similar flight paths in the x, y-plane. The influence of the differing densities showed up primarily in the x, z-plane, where comparable flight paths occurred for different angles of incidence.

1 Eislage	2 Eistyp y1	2 Eistyp y2	2 Eistyp y3
2	$\alpha \approx 6° \hat{=}$	$\alpha \approx 0° \hat{=}$	$\alpha \approx 2°$
4	$\alpha = 4...6° \hat{=}$	$\alpha \approx 0° \hat{=}$	$\alpha \approx 2°$

Key: 1-ice position 2-ice type

i.e. ice type Y1 ($\gamma \approx 2{,}2$ gr/ cm^3) at $\alpha \approx 6°$ had a similar flight path profile as ice type Y2 ($\gamma \approx 0{,}5$ gr/cm^3) at $\alpha = 0°$ or ice type Y3 ($\gamma \approx 1{,}2$ gr/ cm^3) at $\alpha \approx 2°$.

4.3 Ice Separation from the Wing

The performed tests showed that on the wing intake side in the range of 0% to about 1% L(y) breaking ice can lead to damage to the engines.

Due to the underpressure prevailing at these places, the "ice particles" are lifted up and frequently fly:

a) just under the engine gondola

b) against or beside the gondola, or

c) into the engine gondola. A tabular evaluation of measurements is presented in pages 56-59.

1 Eisnase	2 Eistyp	MR	α	β	q_∞	Proto-koll-Nr 3	Bild 4 veränd.	Flugbahn der abgelösten Eisteilchen 7: in die TW-Gondel 5	gegen oder seitlich neben TW 8	unter TW 9	Sonder durch 10	sitzt auf Flügel (Stup.) 11	unter Flügel durch 12
%	%	%	°	°	kp/m²	%	%						
3a	X7	4284	0	0	42	92-31A	nein 6					X	
	X7	4278				90-15						X	
	X11					91-02							X
						90-07							X
	X11					91-03						X	
	X14	4278	0	0	42	91-22	nein 6					X	
	X11	4278	0.5	0	42	91-5	ja 16		X				
	X7	4278	2	0	42	90-19	nein 6					X	
		4284			42	92-32A	ja 16			X			
	X7	4284			85	93-3	nein 6					X	
	X8	4278			42	90-21	nein 6					X	
	X9					90-25	ja 16	X					
	X10					90-28	nein 6					X	
	X10	4278	2	0	42	90-32	nein 6					X	
3a	X14	4278	2.5	0	42	91-23	ja 16	X					

Key: 1-ice pos. 2-ice type 3-log
4-picture avail. 5-into the 6-no
7-flight path of separated ice
particle 8-against 9-under 10-sits
on 11-engine gondola 12-next to
engine 13-through engine gondola
14-wing (stag. pt.) 15-through
wing 16-yes

VEREINIGTE FLUGTECHNISCHE WERKE-FOCKE-WULF GMBH BREMEN

WX 75-13

614 Ice Separation From Wing

1 Eisart	2 Eistyp	MR	α	β	q∞	Proto-3 koll-Nr	Bild4 vorhanden	Flugbahn der abgelösten Eisteilchen 7					
								in Strut	gegen 8 oder dicht neben TW	unter 9 TW - 11 Gondel	durch Gondel 13	sitzt fest (Flügel 14 Strut.)	unter 9 Flügel 15 durch
/	/	/	°	°	kp/in²	/	/						
3a	X1	4268	4	0	42	88-1	ja 16	X					
	X3	4272				89-30	nein 6	-	-	-	-	-	-
	X7	4278			42	90-20	ja 16		X				
	X7	4284			85	93-4			X				
	X8	4278			42	90-22				X			
	X10					90-29			X				
3a	X10	4278	4	0	42	90-33	ja 16		X				
3a	X7	4284	0	0	85	93-7	nein 6					X	
	X11	4278			≈20	91-7	nein 6			X			
	X13				42	91-13	ja 16	X					
	X14				≈35	91-14	nein 6			X			
	X14				42	91-20	ja 16			X			
	X11	4278	0	0	42	90-08	nein 6			X			
	X3	4272	0,5	0	42	88-23	nein 6			X			
	X5	4284			85	93-13		X					
	X7	4284			85	93-08				X			
3a	X14	4278	0,5	0	42	91-21	nein 6	X					

Key: 1-ice pos. 2-ice type 3-log 4-picture avail. 5-into the 6-no 7-flight path of separated ice particle 8-against 9-under 10sits on 11-engine gondola 12-next to engine 13-through engine gondola 14-wing (stag. pt.) 15-through wing 16-yes

NASA CR-179
WX 75-13

614 Ice Separation from Wing

1 Eisnge	2 Eistyp	MR	α	β	q_∞	3 Proto Koll-Nr	4 Bild vorhanden	Flugbahn der abgelösten Eisteilchen 7					
								in 5 Sie	gegen 8 oder nicht neben TW	unter 9 TW-Gon-	sirzaus 10 Flügel (Stagn.)	unter 11 Flügel durch	
%	%	%	°	°	kp/in²	%	%	TW - 11 Gondel		del durch 13			
3a	X1	4272	2	5	42	89-12	ja 16	X					
	X11	4278	2	0	42	90-11	nein 6	X					
	X2	4268	4	0	42	88-9	ja 16			X			
3g	X12	4278	4	0	42	91-12	nein 6			X			
3f	X11	4278	1.5	0	42	91-06	nein 6					X	
	X7	4284	2	0	42	92-35A	ja 16				X		
	X7	4284	2	0	85	92-34A	ja 16				X		
	X1	4268	4	0	42	88-07	ja 16				X		
	X7	4284	4	0	85	92-37A	nein 6					X	
3f	X1	4268	6	0	42	88-03	ja 16	X					

Key: 1-ice pos. 2-ice type 3-log 4-picture avail. 5-into the 6-no 7-flight path of separated ice particle 8-against 9-under 10-str on 11-engine gondola 12-next to engine 13-through engine gondola 14-wing (stag. pt.) 15-through wing 16-yes

VEREINIGTE FLUGTECHNISCHE WERKE-FOKKER GMBH

WX 75-13

WX 75-13

614 Ice Separation From Wing

Blatt:

Eislage [1]	Eistyp [2]	MR	α	β	q_∞	Protokoll-Nr [3]	Bild vorhanden [4]	Flugbahn der abgelösten Eisteilchen [7]: in [5] TW-Gondel [11]	gegen [8] / dicht neben TW [12]	unter [9] TW-Gondel durch [13]	sitzt auf [10] Flügel (Staup.) [14]	unter [9] Flügel durch [15]	
./.	./.	./.	°	°	kp/m²	./.	./.						
3b	X7	4234	0	0	85	93-10	ja [16]				X		
	X7	4234	2	0	85	93-11	ja [16]				X		
	X1	4268	4	0	42	88-02	ja [16]	X					
	X2	4268	—	—	100	88-10	ja [16]		X				
3b	X7	4234	4	0	85	93-12	nein [6]			X			
3c	X1	4268	4	0	42	88-04	ja [16]				X		
3c	X1	4268	6	0	42	88-05	ja [16]				X		
3d	X1	4268	4	0	42	88-03	ja [16]			X			
3e	X1	4268	4	0	42	88-06	ja [16]					X	

Key: 1-ice pos. 2-ice type 3-log 4-picture avail. 5-into the 6-no 7-flight path of separated ice par particle 8-against 9-under 10-sits on 11-engine gondola 12-next to engine 13-through engine gondola 14-wing (stag. pt.) 15-through wing 16-yes

1 Lage	Gefährdung des Triebwerkes bei $\alpha_K = -6°$ 2
3a 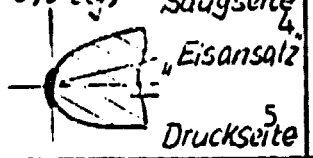	6 groß ($_{10}$bei $\alpha_M \approx 2 \ldots 4°$)
3g 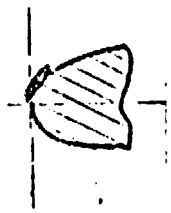	6 groß ($_{10}$bei $\alpha_M \approx 0 \ldots 4°$)
3b 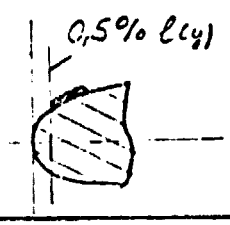	7 mäßig ($_{10}$bei $\alpha_M \approx 3 \ldots 4°$)
3d 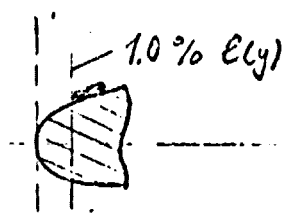	8 gering ($_{10}$bei $\alpha_M \approx 2 \ldots 3°$)
3f 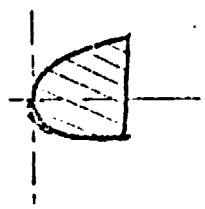	7 mäßig ($_{10}$bei $\alpha_M > 4°$)
3c 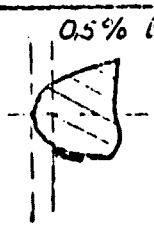	8 gering ($_{10}$bei $\alpha_M > 6°$)
3e 	9 keine

The presentation below is a rough compilation of results from photo and test record evaluation.

Key: 1-position
2-danger to the engine
3-intake side
4-"ice blocks"
5-pressure side
6-great
7-moderate
8-low
9-none
10-at

4.4 Determination of the Average Ice Particle Velocity when Separated from the Fuselage

From the spacing of two ice particles, the average velocity between these positions can be roughly calculated if the transit time is known.

By neglecting the particle acceleration:

$$v = \frac{ds}{dt} \quad \text{or} \quad v_m = \frac{\Delta s}{\Delta t}$$

Here:

1. $\Delta s = m \cdot \Delta s' \; [m]$

m = scale factor photo/model test

$\Delta s'$ = spacing of two particle positions on the photo

Δs = spacing of two particle positions in the model test

2. $t = \frac{1}{f} \; [s]$

f = stroboscope flash frequency

$$\boxed{v_m = m \cdot \Delta s' \cdot f \; [m/s]}$$

A compilation of the determined particle velocities for QE 8892 (≙ wing front edge in the engine region) is found in pages 63-65.

The overview below gives some indication of the influence of angle of incidence, sideslip angle, "ice position" and "ice type".

In summary, we can say that

1. The influence of angle of incidence could not be determined for the small number of flight path photos.

2. The particles separating in the cockpit region have a somewhat greater speed at the front wing edge than the "radome particles".

1	2			v_m/v_∞
1				≈ 0,23
				0,26/0,27
				≈ 0,27
2	y1			0,21/0,20 bis 0,25
				0,21...0,26
				0,25...0,26
				0,20/0,27 bis 0,29
				0,20...0,23
	y3			0,41...0,44
				0,31...0,37
4	y1			0,23/0,25 bis 0,27/0,31
				≈ 0,29
				≈ 0,25
				0,32...0,53
				0,32...0,34

Key: 1-ice position 2-ice type

3. No significant influence of sideslip angle could be determined in the existing flight path photos.
   Trend: $\beta > 0° \Rightarrow v_\beta > v_{\beta=0°}$

4. The influence of stagnation pressure on the velocity ratio v_m/v_∞, due to the relatively large stagnation width of the few measured values, could not be determined.

5. The small-density test bodies attain greater velocities at about the same geometric dimensions.

A rough determination of the kinetic energies of the various test bodies shows that they are on the same magnitude:

$$E_{kin} = \frac{m}{2} v^2$$

$$\frac{E_{kin\ Y1}}{E_{kin\ Y2}} \approx \frac{E_{kin\ Y2}}{E_{kin\ Y3}} \approx \frac{E_{kin\ Y1}}{E_{kin\ Y3}} \approx 1$$

E 614 Ice Separation from the Fuse-lage. Determination of average ice particle velocity at (a leading wing edge in engine area

(1)	(2)	(3)	(4)	(5)	(6)	(7)	(8)	(9)	(10)	(11)	(12)	(13)	
ice pos.	ice type	MP	α	β	q_∞	v_∞	m	f	$\Delta s'$	Δs	v_m	v_m/v_∞	
							(8)·(9)	(10)·(9)	(11)·(9)	(12)/(6)			
/	/	/	°	°	kp/m²	m/s	/	1/s	m	m	m/s	/	
1	41	4258	12	0	42	≈ 253	3,33	100	0,018	0,060	6,0	0,23	
		4259	14	0			3,33		0,018	0,060	6,0	0,23	
		4261	12	5			3,33		0,020	0,067	6,7	0,25	
		4261	14	5			3,33		0,021	0,070	7,0	0,27	
1	41	4259	14	-5	42	≈ 259	3,33	100	0,019	0,063	6,3	0,24	
2	41	4262	0	0	42	≈ 259	3,51	100	0,016	0,054	5,4	0,21	
		4281	0	0	85	≈ 364	5,55		0,017	0,094	9,4	0,25	
		4281	0		100	≈ 400	3,70		0,017	0,063	6,3	0,16	
		4262	2		42	≈ 259	5,71		0,012	0,068	6,8	0,26	
		4266	2		100	≈ 400	5,71		0,019	0,073	8,3	0,24	
		4268	4		100	≈ 400	5,71		0,018	0,103	10,3	0,26	
		4268	4	0	42	≈ 259	5,71		0,017	0,066	6,6	0,25	
		4267	0	5			6,25		0,012	0,025	2,5	0,09	
		4263	2	5			3,57		0,015	0,053	5,3	0,20	
		4267	2	5			5,55		0,012	0,071	7,1	0,27	
		4269	4	5			5,55		0,012	0,011	2,1	0,08	
		4264	2	-5			3,57		0,015	0,053	5,3	0,20	
2	41	4265	2	-5	42	≈ 259	5,51	100	0,011	0,061	6,1	0,23	
2	42	4273	0	0	42	≈ 259	5,71	100	0,020	0,105	10,5	0,41	
		4283	0	0	42	≈ 259	5,41		0,021	0,114	11,4	0,44	
2	42	4283	0	0	85	≈ 364	5,41	100	0,029	0,151	15,1	0,43	

614 - Eisablösung am Rumpf
Ermittlung der mittleren Eisteilchengeschwindigkeit

WX 75-13

614--Ice Separation from the Fuselage. Determination of average ice particle velocity at QF = 8892 (≙ leading wing edge in engine area

①	②	③	④	⑤	⑥	⑦	⑧	⑨	⑩	⑪	⑫	⑬
Ice pcs	Ice type	MP	α	β	p_∞	v_∞	m	f	Δs'	Δs	$\bar{v}_m$	v_m/v_{ice}
			°	°	kp/m²	m/s		1/s	m	m	m/s	
1	42	4225	4	0	42	≙ 250	5.44	100	0.019	0.125	10.5	0.41
1	43	4250	0	0			3.55		0.022	0.080	8.0	0.31
		4250					3.64		0.023	0.083	8.3	0.32
		4233					5.71		0.015	0.091	9.1	0.35
		4230	0				3.64		0.024	0.094	9.4	0.36
		4230	4				4.22		0.022	0.096	9.6	0.37
		4235	2				5.71		0.015	0.089	8.9	0.34
2	43	4225	4	0	42	≙ 250	5.71	100	0.115	0.088	8.8	0.36
4	41	4250	0	0	42	≙ 250	3.64	100	0.017	0.062	6.2	0.24
		4225			42		5.55		0.010	0.054	5.4	0.25
1		4223			85	≙ 360	3.64		0.028	0.102	10.2	0.28
		4233			100	≙ 400	3.64		0.034	0.124	12.4	0.31
		4233			100	≙ 400	5.55		0.032	0.134	13.4	0.34
		4235	0	0	85	≙ 360	5.55		0.015	0.023	9.2	0.23
		4230	2	5	42	≙ 250	5.55		0.013	0.076	7.6	0.33
	41	4230	2	-5			5.55		0.022	0.085	8.5	0.35
	42	4225	0	0	42	≙ 250	3.64		0.026	0.121	12.1	0.53
		4223	1	1	42		5.55		0.020	0.111	11.1	0.43
		4233			85	≙ 360	5.55		0.025	0.144	14.4	0.39
		4236			85	≙ 360	5.55		0.028	0.155	15.5	0.42
4	42	4230	0	0	150	≙ 400	3.64	150	0.050	0.190	19.0	0.50

614 - Eisablösung am Rumpf
Ermittlung der mittleren Eisteilchengeschwindigkeit

WX 75-13

614--Ice Separation from the Fuselage. Determination of average ice particle velocity at QF = 8892 (≙ leading wing edge in engine area

①	②	③	④	⑤	⑥	⑦	⑧	⑨	⑩	⑪	⑫	⑬
Ice pos.	ice type	hp	α	β	q_∞	v_∞	n	f	$\Delta s'$	Δs	v_m	v_m/v_∞
			°	°	kp/m²	m/s	-	m/s	m	m	m/s	-
1	1	42	0	0	42	≈ 25	3,64	100	0,135	0,138	13,8	0,53
2	1	42	1	1			3,64		0,036	0,131	13,1	0,50
3	1	42	1	1						0,111	11,1	0,43
4	2	42	1	1					0,021	0,117	11,7	0,45
5	3	42	0	1					0,016	0,092	8,9	0,34
6	1	42	4	1					0,015	0,083	8,3	0,32
7	3	42	4	0	42	≈ 25	3,65	100	0,014	0,082	8,3	0,32

ORIGINAL PAGE IS OF POOR QUALITY

5. Summary

The wind tunnel measurements "To Determine Flight paths of Separated Ice Particles" performed with the VFW 614 showed for the studied flight status:

$$\begin{aligned} \text{Elevation} &\approx 6000 \text{ ft} \\ v_\infty &\approx 200 \text{ kts} \\ \gamma_K &= -6^\circ \\ \alpha &\approx 0 \ldots 4^\circ \\ \beta &\approx 0^\circ \end{aligned}$$

that ice particles released both from the radome and at certain positions of the leading wing edge can be the source of engine damage.

Engine damage through cockpit ice-separation is viewed as unlikely.

For the specific case of simultaneous damage to both engines, as occurred during the VFW 614 Test Flight, a radome ice-separation cannot be entirely excluded as the origin of the damage, but it is viewed as unlikely. The tests showed that only at sideslip angles of $\beta \lesssim 0^\circ$ do the flight paths come near the engine, whereas on the opposing wing side, they run farther to the outside.

In the sketch below we find those ice-separation zones which represent an acute danger for the engines in the studied flight state.

6. Conclusions

In conclusion, it must be expressly pointed out again that the statements on possible engine damage through released ice particles relate exclusively to the assumptions on model status and location of ice separation points in this test.

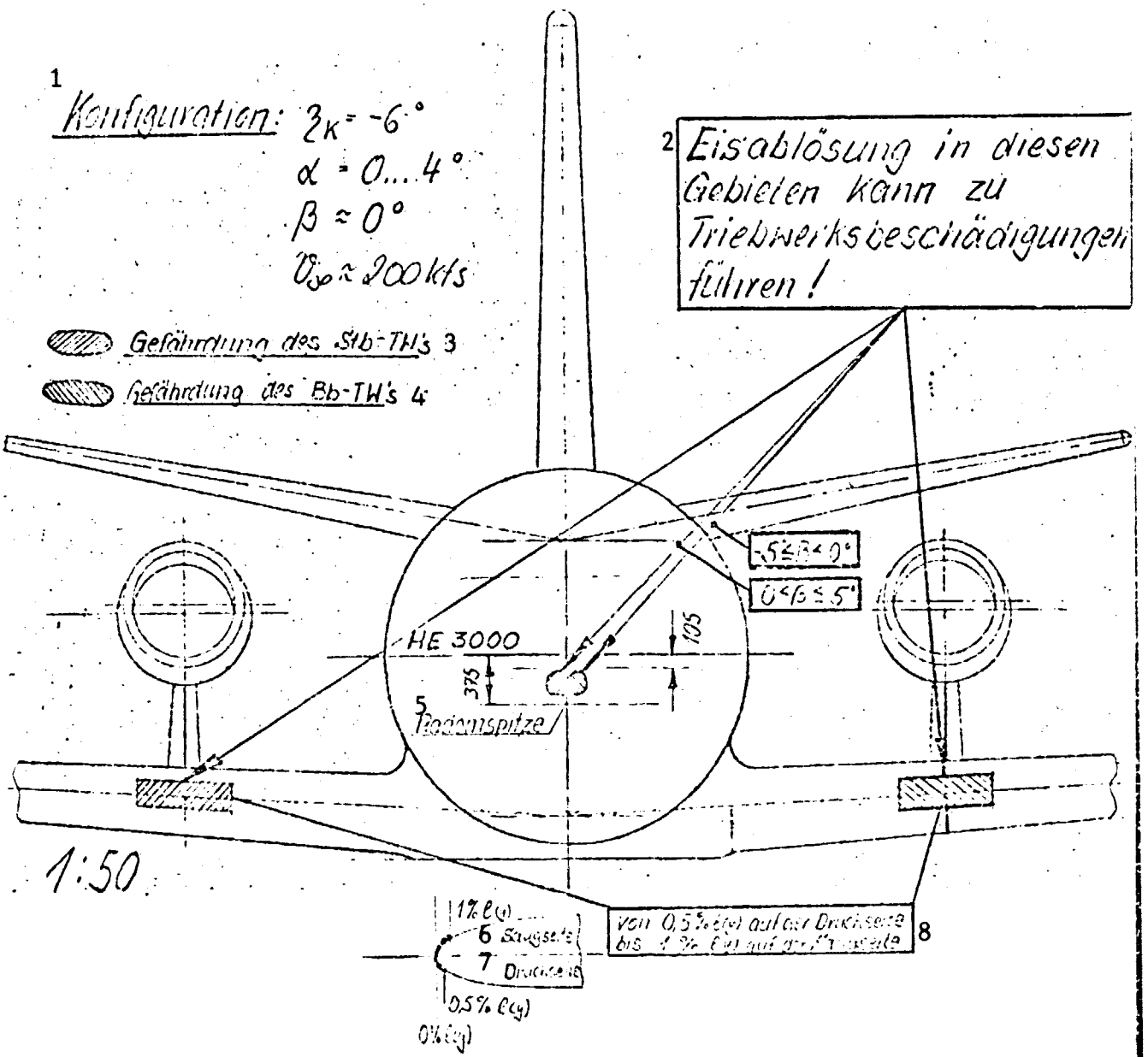

Ice Separation Positions which Can Lead to Damage to the Engines

Key: 1-configuration 2-ice separation in these regions can lead to engine damage 3-danger to the Stb engine 4-danger to the Bb engine 5-radome peak 6-intake side 7-pressure side 8-from 0.5% on the pressure side to 1% on the intake side

Whether ice particles indeed occur at the assumed positions (and also break off) and whether they can cause damage to the engine through their mass, is not the subject here.

But if investigations in this regard should confirm the chosen separation positions, it is suggested: To prevent the generation of ice build-up on the leading wing edge in the engine area by suitable means in any event.

For the case that ice particles separating from the radome or other positions could cause damage due to their size, appropriate wind tunnel investigations should be performed for the flight modes under consideration.

7. Annex

Annex to report EF 586, part 3.

Compilation of flight path photos.

The two existing copies are located at:

1. at Eo 2
2. at the VFW-F wind tunnel

REPORT Ef 586, part 4

Subject: Summary of the Most Important Results of the Wind Tunnel Measurements on the Ice Flight Paths using the VFW 614 Model

Summary: This part of the report gives a rough overview of the results of wind tunnel tests performed on the subject "Ice Flight Paths on the VFW 614".

Since a detailed final report is not yet completed, this summary will serve as a preinformation of the most important results.

Bearbeitet / Prepared	Geprüft / Checked	Gebilligt / Approved	Anerkannt / Acknowledged
J. Anders	J. Anders		

Verteiler / Copy to:	Neuausgabe / Re-issue: Datum / Date:	Bem. / Remarks:
	Änd.-Ausg. / Revision: Seite / Page: Datum / Date:	
Datum/Date: 9.1.76 Ausg./Rev. No.:		Anz. der Seiten: 5 Numb. of Pages:

Contents

1. General Information

Within the frame of investigations on the icing problem of the VFW 614, wind tunnel tests were performed in the VFW-F wind tunnel for the purpose of determining possible flight paths of separating ice. The ice separation was simulated at 4 illustrated positions on the 1:15 scale model.

Pos. 1

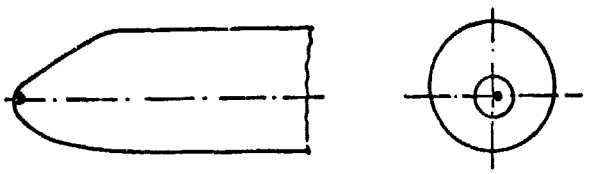

Radome peak

Pos. 2

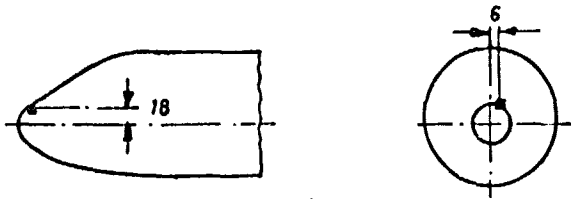

Radome edge

Pos. 3

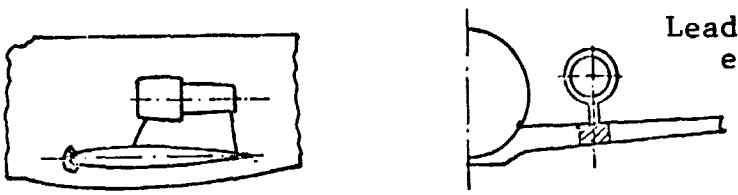

Leading wind edge in the engine area

Pos. 4

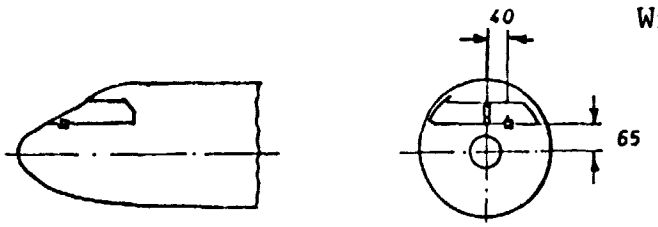

Windshield wiper area

Under consideration of similarity laws (see part 2), the ice separation was simulated via special features on the model and the flight paths of the flying particles were registered photographically. A detailed test description and the evaluation and documentation of all results will appear in a future report.

2. Scope of Testing

In 83 test points, a total of more than 350 flight path tests was performed, of which ca. 200 were registered photographically. The following parameters were varied during the testing:

-angle of incidence α	$0 < \alpha < 14^\circ$
-sideslip angle β	$-5^\circ, 0^\circ, +5^\circ$
-ice separation position	Pos. 1, 2, 3, 4.
-ice shapes	Type x, y
-spec. weight γ	$0,5 < \gamma < 7,8$ gr/cm^3
-incident flow stagnation pressure	q_∞ = 20, 42, 85, 100 kp/m^2

3. Results

3.1 Pos. 1: Radome Peak

The ice separating from the radome peak flys under the wing at an angle of incidence of $0 < \alpha < 10^\circ$. Not until angles of $\alpha > 12^\circ$ are reached do the paths of the ice particles lead into the vicinity of the engine.

3.2 Pos. 2: Radome Edge

The engine lies in the scattering range of ice flying off from this position. At angles of incidence of $\alpha = 0^\circ$ the majority of ice particles flies under the wing. At $\alpha = 4^\circ$, the flight paths lie directly in the engine area, whereas at $\alpha = 6^\circ$, the majority of particles fly off over the engine.

3.3 Pos. 3: Leading Wing Edge in the Engine Area

Simulated ice particles released near the stagnation point of the leading wing edge fly at angles of incidence of $2^\circ < \alpha < 4^\circ$ directly into the engine inlet. In order to eliminate uncertainties in the application of similarity laws, in these tests the important similarity parameter--the specific weight of the particle--was varied. But for all used particle types ($0,5 < \gamma < 7,8$ gr/cm^3) hits in the engine inlet were registered in this flight mode.

3.4 Pos. 4: Windshield Wiper Location

From this position, the ejected particles tend to get into the engine area only at small angles of incidence ($\alpha \rightarrow 0^{\circ}$). At $\alpha > 2^{\circ}$ the flight paths lead out over the engine.

4. Summary

The tests described here have shown that ice forming in and separating from the regions: Radome, leading wing edge in the engine area, windshield wiper, follows flight paths in the flight range under discussion ($0 < \alpha < 4^{\circ}$; $v_{\infty} \approx$ 200 kts) which lead to the immediate vicinity of the engine inlet or directly into the engine.